Electronic Supplementary Material (ESI) for Organic & Biomolecular Chemistry.
This journal is © The Royal Society of Chemistry 2021

supporting information accompanying:

Comparison of $[Pd_2L_4][BF_4]_4$ cages for binding of *n*-octyl glycosides and nitrate (L = isophthalamide or dipicolinamide linked dipyridyl ligand)

Brian J.J. Timmer,[1] , Eduard O. Bobylev[1] and Tiddo J. Mooibroek[1,]*

[1] van 't Hoff Institute for Molecular Sciences, Universiteit van Amsterdam, Science Park 904, 1098 XH Amsterdam, The Netherlands. *Corresponding author e-mail: t.j.mooibroek@uva.nl

Table of Contents

Section S1. Materials and methods **2**
Section S2. Synthetic procedures **3**
Section S2a. Overview of syntheses 3
Section S2b. Synthesis of bidendate dipyridyl ligands **1** and **2** 4
Section S2c. Synthesis and characterizations of Pd complexes 17
Section S3. Titration experiments **29**
Section S3a. Formation of Pd complexes 29
Section S3b. Dilution of Pd complexes 31
Section S3c. Binding studies of $[Pd_2\mathbf{1}_4][BF_4]_4$ 33
Section S3d. Binding studies of $[Pd_2\mathbf{2}_4][BF_4]_4$ 40
Section S4. Computational details **45**
References **49**

Section S1. Materials and methods

All solvents and chemicals were purchased from commercial suppliers and used without further purification. Solvents, when needed, were dried by standard distillation techniques or for larger amounts (>10 mL), the solvent was tapped from a Solvent Purification System (SPS) from mbraun (MB SPS-800, with standard mbraun drying columns). Pyridine and DMF were obtained as 'extra dry' grade in septum sealed bottles and used as received. Reactions were carried out under a Nitrogen atmosphere using standard Schlenk techniques, where dry solvents are specified. Silica gel column chromatography was performed using Silica Gel 60 from Macherey-Nagel (0.040 - 0.063 nm). Bis-ethylester **B**[1] as well as bromide **A** and bis-pentafluorophenyl ester **E**[2] were prepared according to literature procedures. Tetrakis[3,5-bis(trifluoromethyl)phenyl]borate is abbreviated as BAr^F in the text.

Nuclear Magnetic Resonance (NMR) spectra were recorded on a Bruker DRX 500 (125.72 MHz for ^{13}C), Bruker AMX 400 (100.62 MHz for ^{13}C), Bruker DRX 300 (75.48 MHz for ^{13}C) or on a Varian Mercury 300 (75.48 MHz for ^{13}C or 282.32 MHz for ^{19}F) spectrometer at room temperature or specifically specified otherwise. The residual solvent peaks were used as internal standards (^1H: δ 7.26 p.p.m., $^{13}C\{^1H\}$: δ 77.16 p.p.m. for $CDCl_3$; ^1H: δ 5.32 p.p.m., $^{13}C\{^1H\}$: δ 53.84 p.p.m. for CD_2Cl_2; ^1H: δ 2.50 p.p.m., $^{13}C\{^1H\}$: δ 39.52 p.p.m. for DMSO-d_6; ^1H: δ 1.94 p.p.m., $^{13}C\{^1H\}$: δ 1.32 p.p.m. for CD_3CN), while ^{19}F NMR spectra were externally referenced to CF_3COOH (–76.55 p.p.m.). Chemical shifts (δ) are given in parts per million (p.p.m.) and coupling constants (J) are quoted in hertz (Hz). Resonances are described as singlet (s), doublet (d), triplet (t), quartet (q), quintet (quint), a combination thereof, broad singlet (br s) or multiplet (m). High Resolution Mass Spectra (HRMS) of the organic molecules were recorded on a JEOL AccuTOFC-plus JMS-T100LP mass spectrometer, with the indicated ionization method. The high resolution mass spectra of the complexes were recorded after electronspray-ionization using a HR-ToF Bruker Daltonik GmbH (Bremen, Germany) Impact II, an ESI-ToF MS capable of resolution of at least 40000 FWHM, which was coupled to a Bruker cryo-spray unit. Detection was in positive-ion mode and the source voltage was between 4 and 6 kV. The sample was introduced with a syringe pump at a flow rate of 18 ul/hr. The drying gas (N_2) was held at 40°C and the spray gas was held at 60°C. The machine was calibrated prior to every experiment via direct infusion of a TFA-Na solution, which provided a m/z range of singly charged peaks up to 3500 Da in both ion modes. Software acquisition Compass 2.0 for Otof series. Software processing m- mass.

^1H NMR titrations were performed using a Bruker DRX 500 spectrometer operating at 298 K or specifically specified otherwise. The titrations were performed by titrating a solution of carbohydrate or nitrate salt to a solution containing freshly prepared Pd-complex. The carbohydrates **3**, **4** and **6** were purified by silica gel column chromatography prior to use (using acetone as the eluent, the column was first thoroughly flushed with the solvent). Association constants (K_a) were determined by monitoring the change in chemical shift (Δδ) for (a) selected proton resonance(s) of a Pd complex and fitting these shifts to a binding model using HypNMR.[3] An estimated goodness of fit was calculated as r^2 from all the observed and fitted Δδ values used in HypNMR. The titration data with glycosides *fitted* very well to a 1:1 model when using the data until about 25 mM glycodise. When using the full concentration range (~150 mM), the 1:1 model failed. Fitting the data to a 1:2 model also did not work out (not shown). The data could be reasonably *modelled* with a 1:3 stoichiometry with very weak 1:2 and 1:3 binding. The exact values for $K_a^{1:2}$ and $K_a^{1:3}$ had little impact on r^2 of the model in the range 2–5 M^{-1} and it was decided to model both as the same constant at ~3 M^{-1}. As we could not genuinely fit these 1:2 and 1:3 constants and because we suspect the shifts may in part be due to polarity effects at elevated levels of glycoside, we do not report these stoichiometries in the main text. Moreover, the $K_a^{1:1}$ obtained from the *fit* to a 1:1 stoichiometry (with data until 25 mM glucoside) and obtained from modelling to a 1:3 stoichiometry (data until ~150 mM glycoside) were nearly identical. For completeness, we do show these 1:3 models alongside the data here in the supporting information.

Section S2. Synthetic procedures

Section S2a. Overview of syntheses

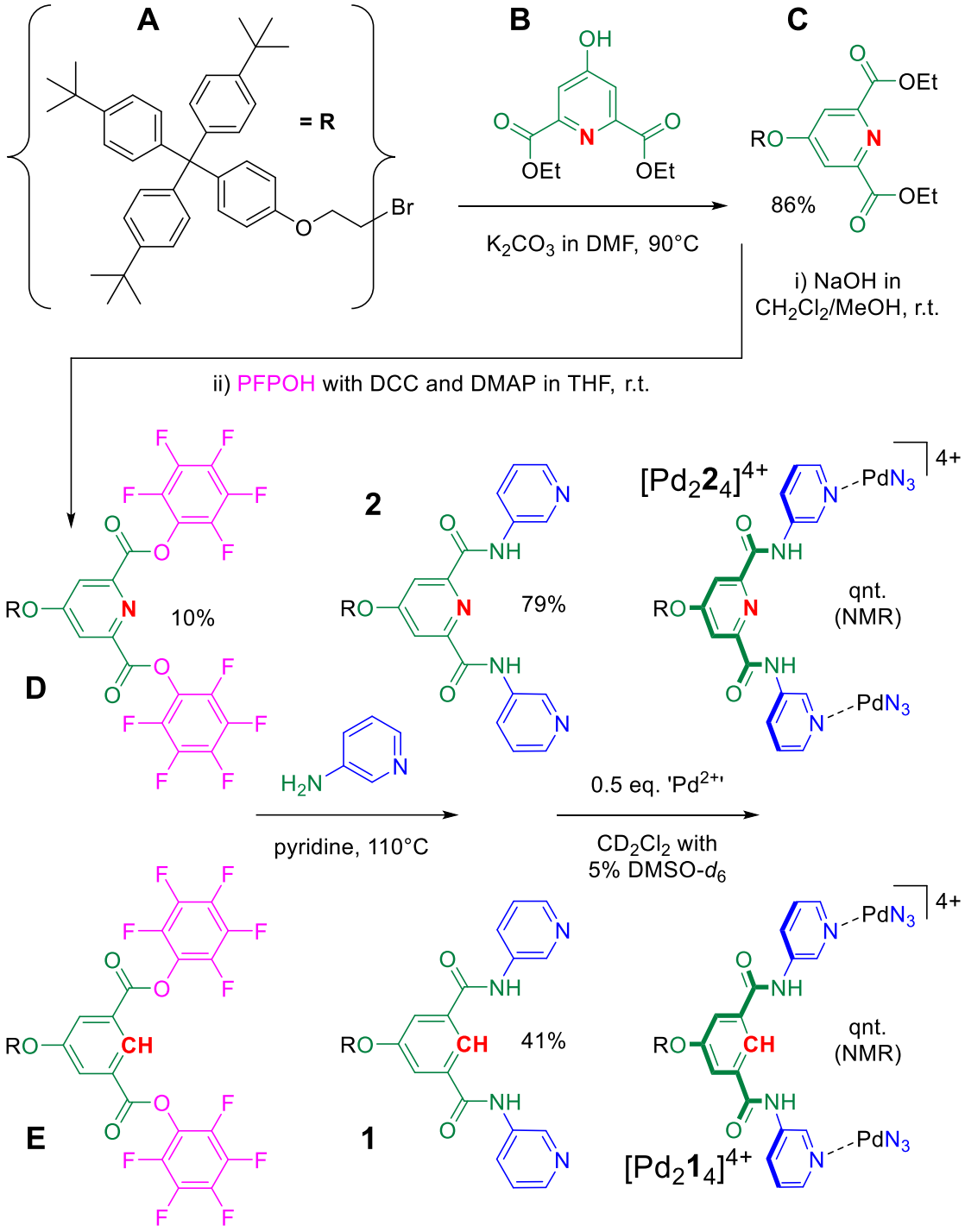

Scheme S1. Overview of the synthetic pathway towards bidentate dipyridyl ligands **1** and **2** and their Pd(ii) complexes. Compound **B**,[1] and **A** and **E**[2] were prepared using literature procedures.

Section S2b. Synthesis of bidendate dipyridyl ligands 1 and 2

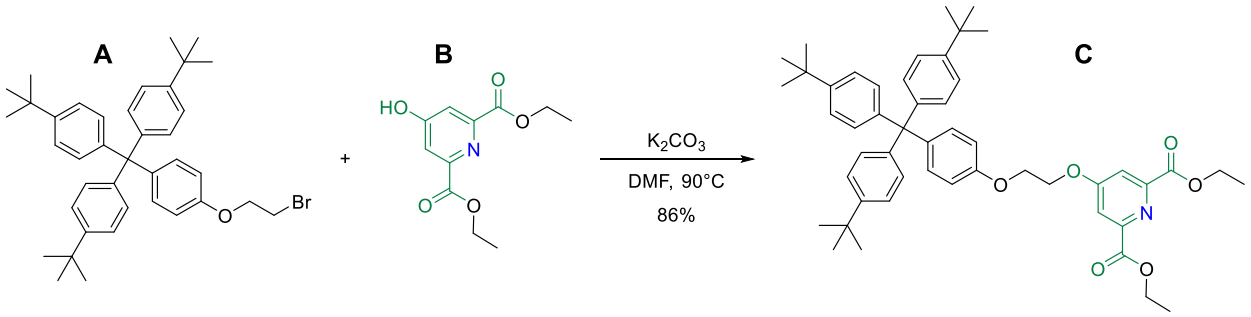

Bis-ethylester C. Bromide **A**[2] (1.0 eq., 5.0 mmol, 3.06 g), alcohol **B**[1] (1.2 eq., 6.0 mmol, 1.44 g) and K_2CO_3 (3.0 eq., 15.0 mmol, 2.07 g) were placed in a Schlenk flask. Dry DMF (60 mL) was added and the reaction mixture was heated to 90°C for 18 h. After cooling to room temperature the solvent was removed by rotary evaporation. The residue was triturated with water and the solids were collected by filtration. The solids were dissolved in CH_2Cl_2 and dried over Na_2SO_4, filtered and concentrated *in vacuo*. The residue was further purified by column chromatography (1:1 PE 40-60/CH_2Cl_2 to CH_2Cl_2 to 5% EtOAc) to afford the product **C** (3.33 g, 4.3 mmol, 86%) as white solid.

^{1}H NMR (500 MHz, $CDCl_3$) δ 7.86 (s, 2H), 7.23 (d, *J* = 7.8 Hz, 6H), 7.14 – 6.99 (m, 8H), 6.80 (d, *J* = 8.2 Hz, 2H), 4.65 – 4.40 (m, 6H), 4.35 (s, 2H), 1.45 (t, *J* = 6.7 Hz, 6H), 1.30 (s, 27H). **^{13}C NMR** (126 MHz, $CDCl_3$) δ 166.81, 164.81, 156.15, 150.40, 148.52, 144.16, 140.61, 132.54, 130.84, 124.22, 114.59, 113.18, 67.50, 65.89, 63.21, 62.56, 34.44, 31.52, 14.35. **MS** (MS FD+ eiFi, m/z) calc. for $C_{50}H_{59}N_1O_6$ $[M]^+$: 769.4342, found:769.4350.

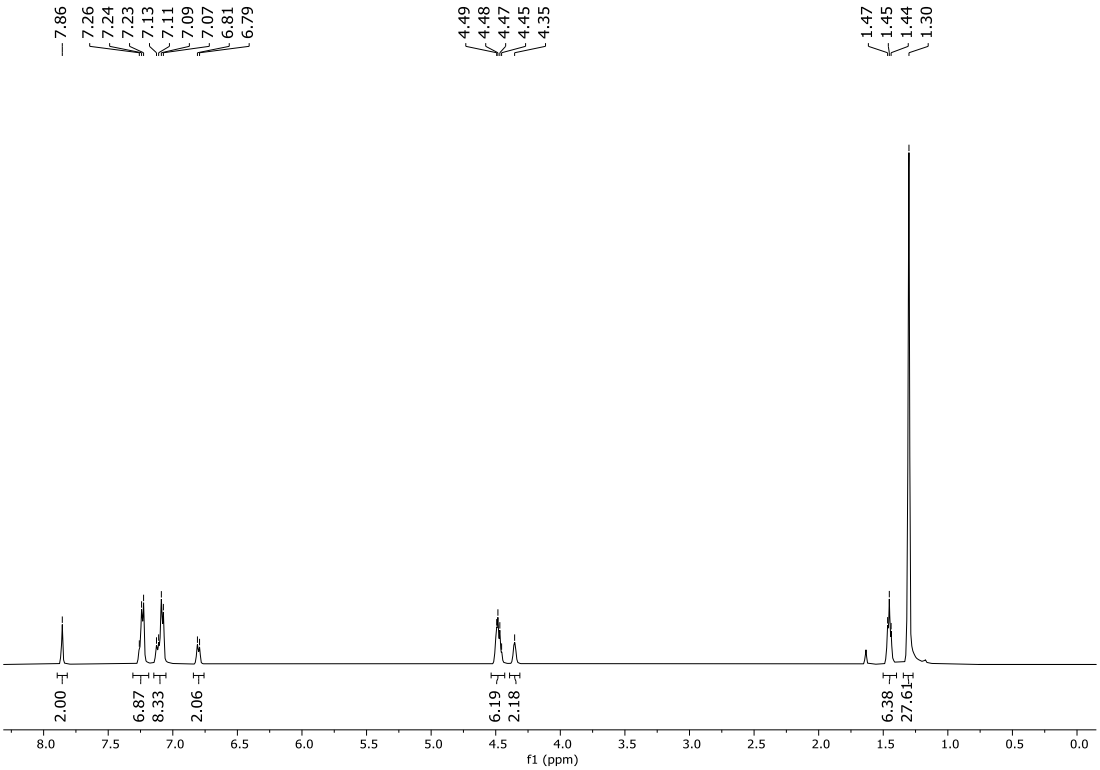

Figure S1. ^{1}H NMR spectrum of bis-ethylester **C** in $CDCl_3$.

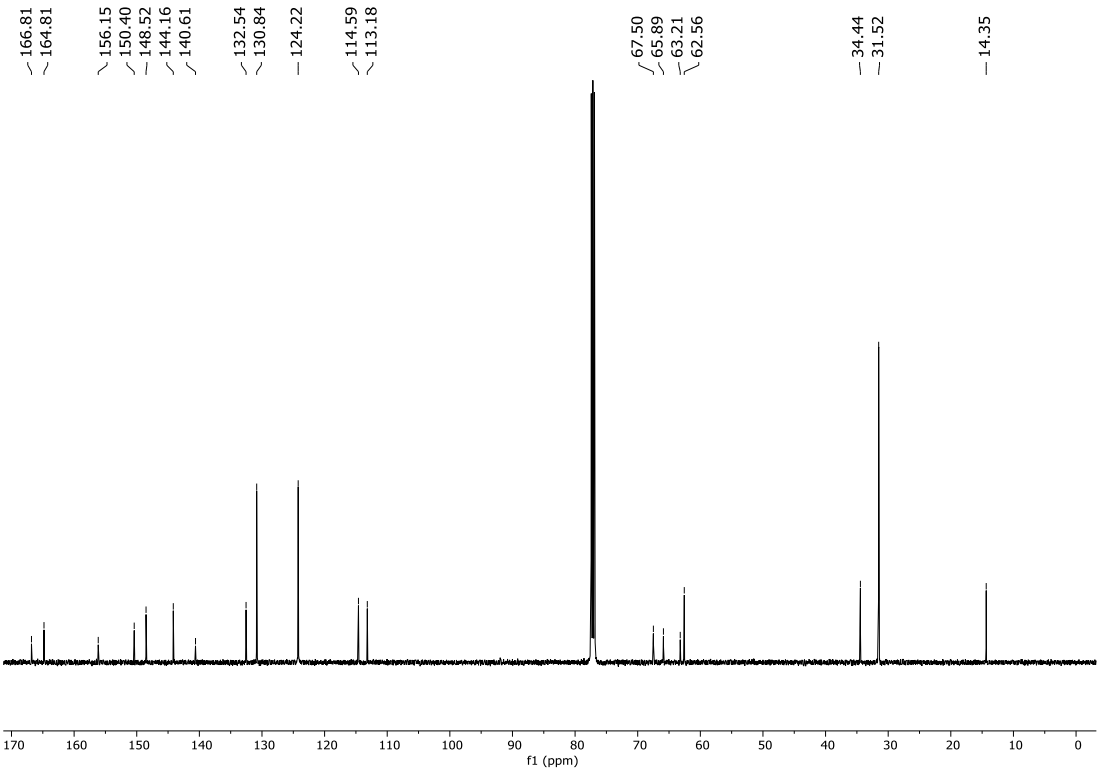

Figure S2. ^{13}C NMR spectrum of bis-ethylester **C** in $CDCl_3$.

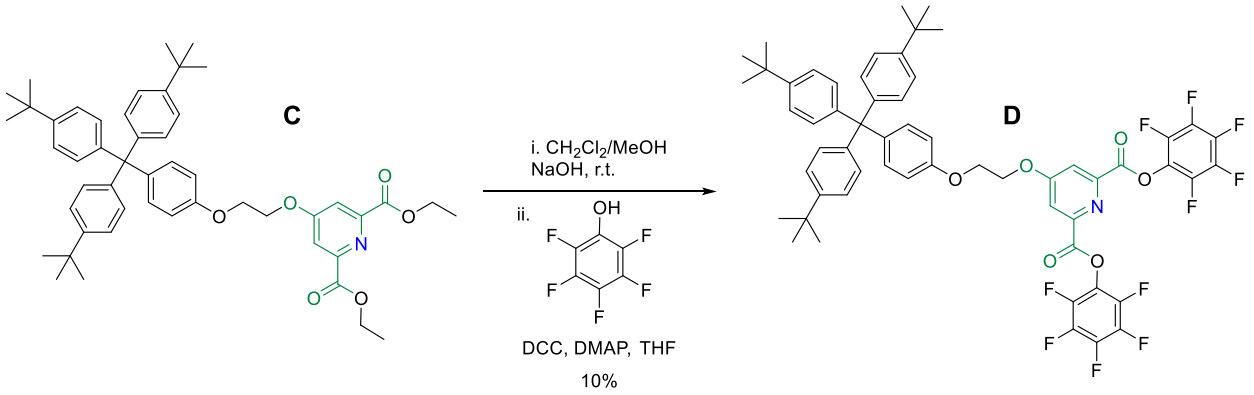

Bis-pentafluorphenyl ester D. Bis-ethylester **C** (1.0 eq., 4.3 mmol, 3.33 g) was dissolved in a mixture of CH_2Cl_2 (45 mL) and MeOH (5 mL) and ground NaOH (10.0 eq., 43.0 mmol, 1.72 g) was added portionwise. After stirring for 16h the solvent was removed by rotary evaporation and the residue was resuspended in CH_2Cl_2. The solution was brought to pH 7 by addition of HCl (1M in H_2O) after which the CH_2Cl_2 was removed by rotary evaporation. The resulting white solids (2.76 g, theoretically 3.89 mmol, 91%) were collected by filtration and dried *in vacuo* at 80°C. Due to insolubility of this diacid the compound was directly used in the following step without further characterization. The (presumed) diacid (2.75 g, 3.85 mmol) was suspended in dry THF (60 mL) containing pentafluorophenol (2.5 eq., 9.63 mmol, 1.77 g). The mixture was cooled to 0°C and a solution of N,N'-dicyclohexylcarbodiimide (DCC, 2.5 eq., 9.63 mmol, 1.99 g) in dry THF (20 mL) was added portionwise. A few minutes after complete addition, 4-dimethylaminopyridine (DMAP, 5 mol%, 0.19 mmol, 23.5 mg) was added and the ice bath was removed. After stirring for 16h the reaction mixture was filtered and concentrated *in vacuo*. The residue was dried on SiO_2 and purified by column chromatography (2:1 to 1:1 PE 40-60/CH_2Cl_2) to afford the product as crystalline white solid (400 mg, 0.38 mmol, 10%). **NB**: product **D** readily hydrolyses in the presence of H_2O and undergoes transesterification in the presence of alcohols *e.g.*, MeOH.

^{1}H NMR (500 MHz, CD_2Cl_2) δ 8.13 (s, 2H), 7.27 (d, *J* = 8.5 Hz, 6H), 7.21 – 7.09 (m, 8H), 6.82 (d, *J* = 8.8 Hz, 2H), 4.60 (s, 2H), 4.41 (d, *J* = 2.2 Hz, 2H), 1.30 (s, 27H). **^{13}C NMR** (126 MHz, CD_2Cl_2) δ 167.73, 160.86, 156.43, 148.90, 147.90, 144.77, 142.68, 141.07, 140.60, 139.50, 137.47, 132.49, 130.79, 125.56, 124.73, 117.54, 113.63, 68.60, 66.38, 63.53, 34.60, 31.47. **^{19}F NMR** (282 MHz, CD_2Cl_2) δ -152.49 (d, *J* = 17.2 Hz), -157.91 (t, *J* = 21.6 Hz), -162.58 (dd, *J* = 21.6, 17.2 Hz). **MS** (MS FD+ eiFi, m/z) calc. for $C_{58}H_{49}F_{10}N_1O_6$ $[M]^+$: 1045.3400, found:1045.3348.

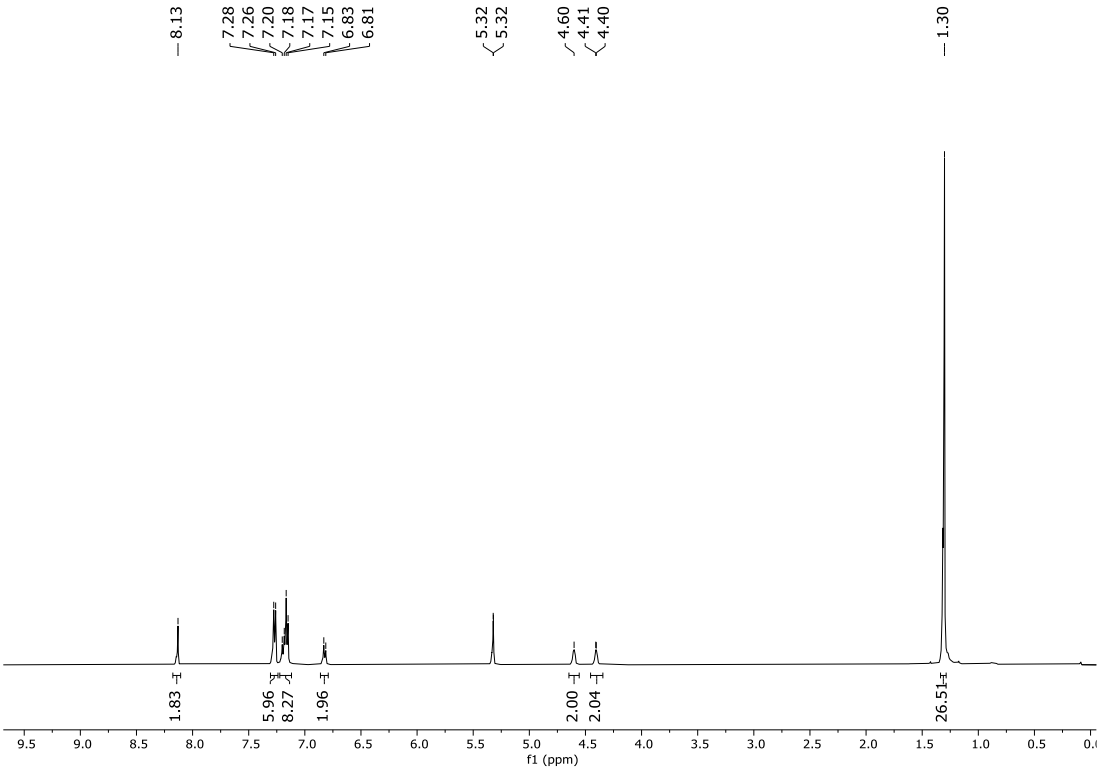

Figure S3. ^{1}H NMR spectrum of bis-pentafluorophenyl ester **D** in CD_2Cl_2.

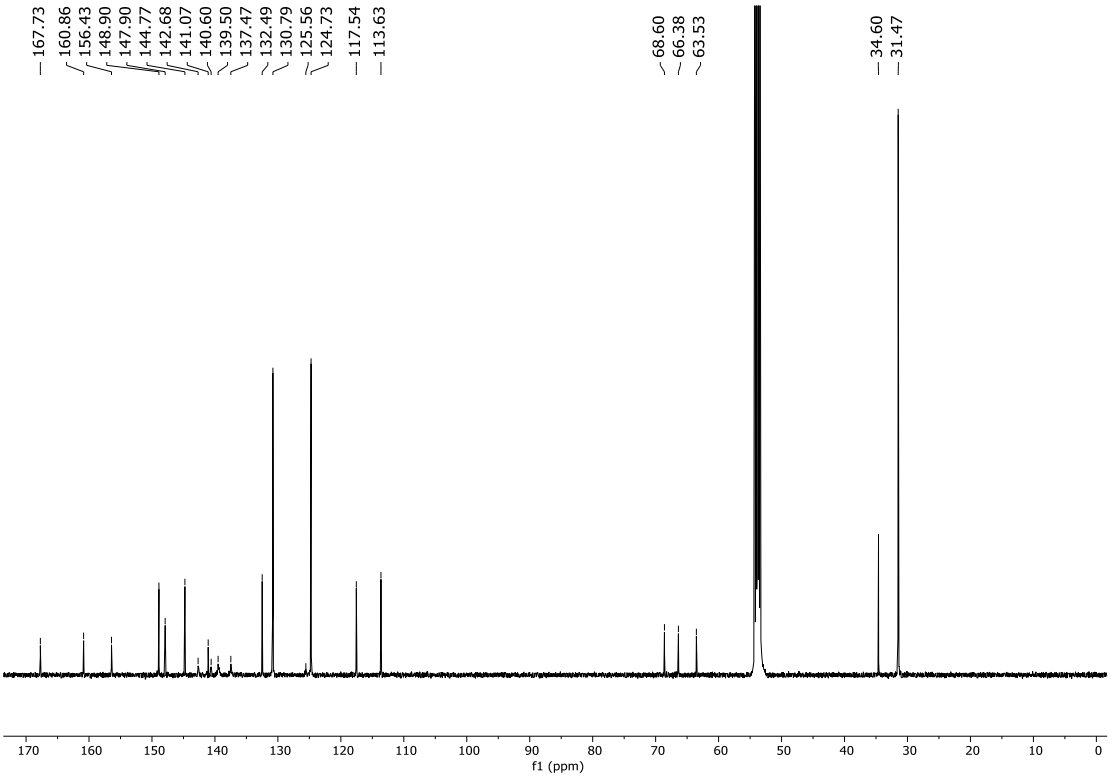

Figure S4. ^{13}C NMR spectrum of bis-pentafluorophenyl ester **D** in CD_2Cl_2.

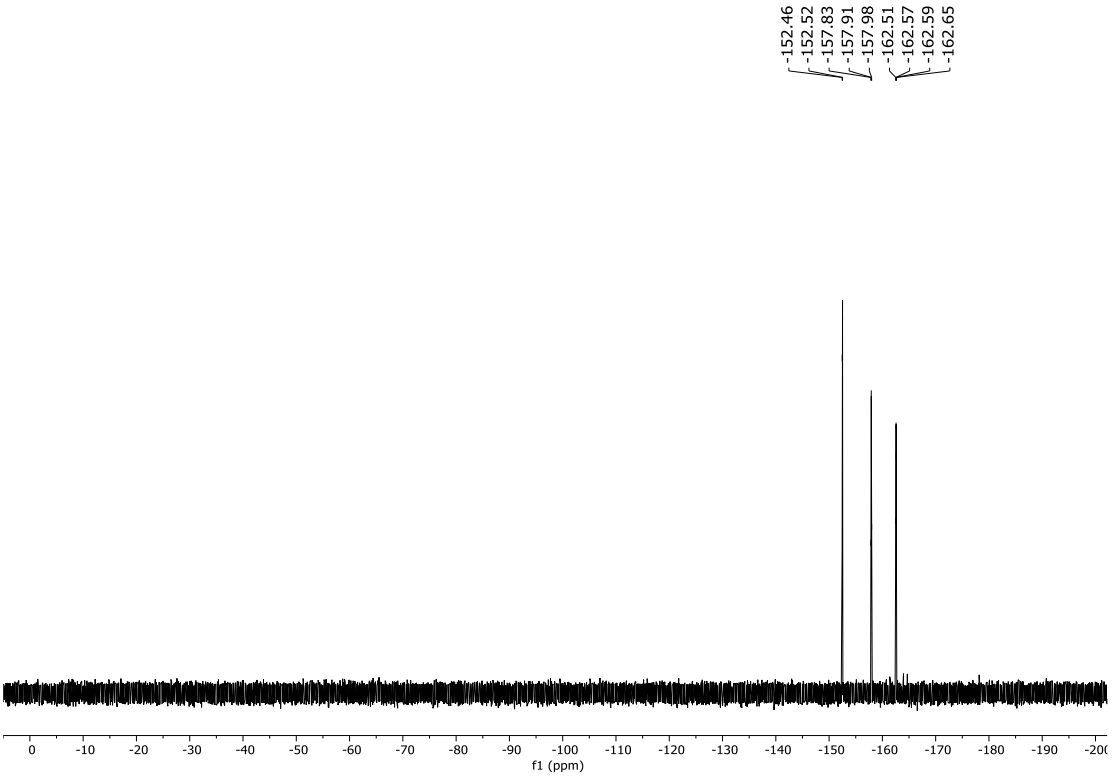

Figure S5. ^{19}F NMR spectrum of bis-pentafluorophenyl ester **D** in CD_2Cl_2.

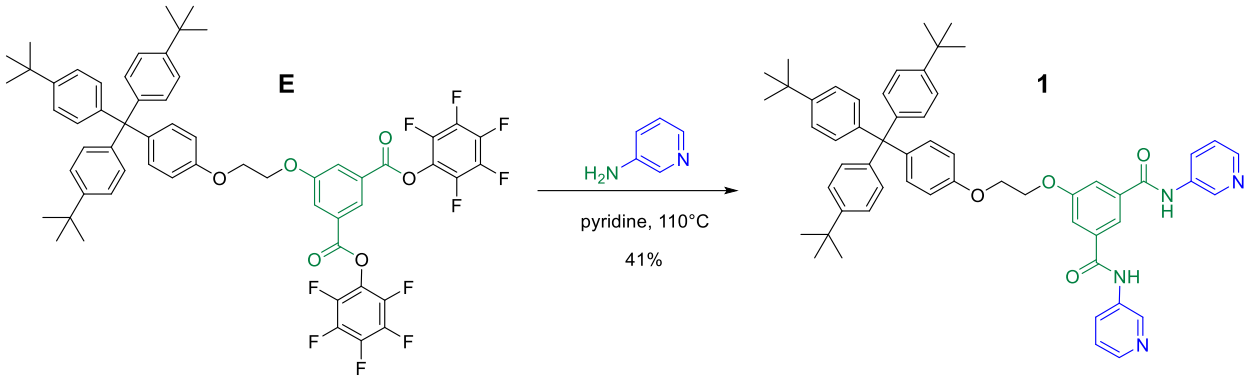

Dipyridyl ligand 1. Bis-pentafuorophenyl ester **F**[2] (1.0 eq., 0.5 mmol, 523 mg), 3-aminopyridine (40 eq., 20.0 mmol, 1882 mg) and dry pyridine (5 mL) were mixed in a Schlenk flask. The mixture was heated to 110°C and stirred for 17h. After cooling to room temperature the pyridine was evaporated by rotary evaporation. The residue was redissolved in CH_2Cl_2 (50 mL) and washed with H_2O (50 mL) and brine (50 mL). The organic layer was dried over Na_2SO_4, filtered and concentrated *in vacuo*. The residue was further purified by flash column chromatography (CH_2Cl_2 to 5% MeOH in CH_2Cl_2). Fractions containing the product were concentrated *in vacuo*. The residual solids were triturated with MeOH and filtered to afford dipyridyl ligand **1** (176 mg, 0.2 mmol, 41%) as white solid.

^{1}H NMR (300 MHz, 10% dmso-d_6 in CD_2Cl_2) δ 10.01 (s, 2H, s3-NH), 8.92 (s, 2H, p2), 8.31 (d, *J* = 4.0 Hz, 2H, p3), 8.27 (ddd, *J* = 8.4, 2.4, 1.5 Hz, 2H, p5), 8.23 (s, 2H, s4), 7.79 (d, *J* = 1.3 Hz, 2H, s2), 7.36 – 7.21 (m, 8H, p4 and d10), 7.21 – 7.09 (m, 8H, d5 and d9), 6.82 (d, *J* = 8.9 Hz, 2H, d4), 4.46 (dd, *J* = 5.6, 2.9 Hz, 2H, d1), 4.34 (dd, *J* = 5.4, 3.1 Hz, 2H, d2), 1.28 (s, 27H, d13). **^{13}C NMR** (75 MHz, 10% dmso-d_6 in CD_2Cl_2) δ 165.65 (s3-CO), 159.25 (s1), 156.66 (d3), 148.73 (d11), 145.31 (p3), 144.72 (d8), 142.65 (p2), 140.57 (d6), 136.59 (s3), 136.15 (p1), 132.35 (d5), 130.71 (d9), 127.79 (p5), 124.61 (d10), 123.66 (p4), 119.81 (s4), 117.66 (s2), 113.55 (d4), 67.54 (d1), 66.71 (d2), 63.41 (d7), 34.51 (d12), 31.41 (d13). **MS** (MS FD+ eiFi, m/z) calc. for $C_{57}H_{60}N_4O_4$ $[M]^+$: 864.4615, found: 864.4618.

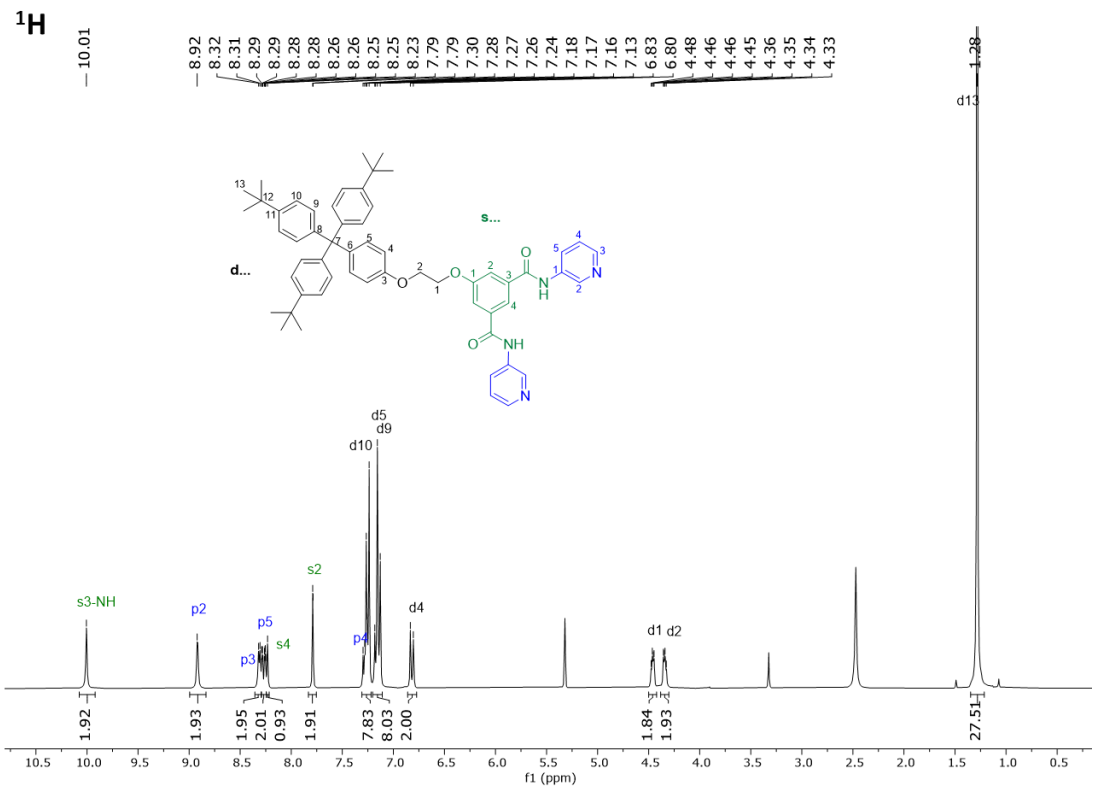

Figure S6. ^{1}H NMR spectrum of dipyridyl ligand **1** in CD_2Cl_2 with 10% dmso-d_6, fully assigned.

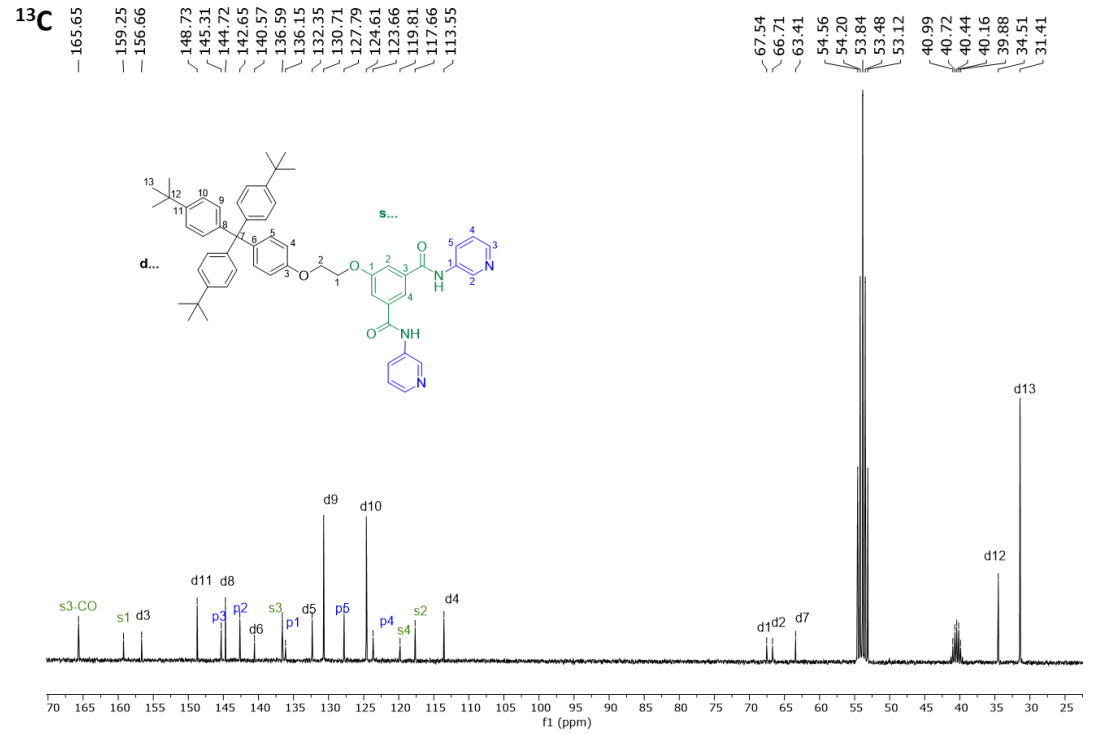

Figure S7. ^{13}C NMR spectrum of dipyridyl ligand **6** in CD_2Cl_2 with 10% dmso-d_6, fully assigned.

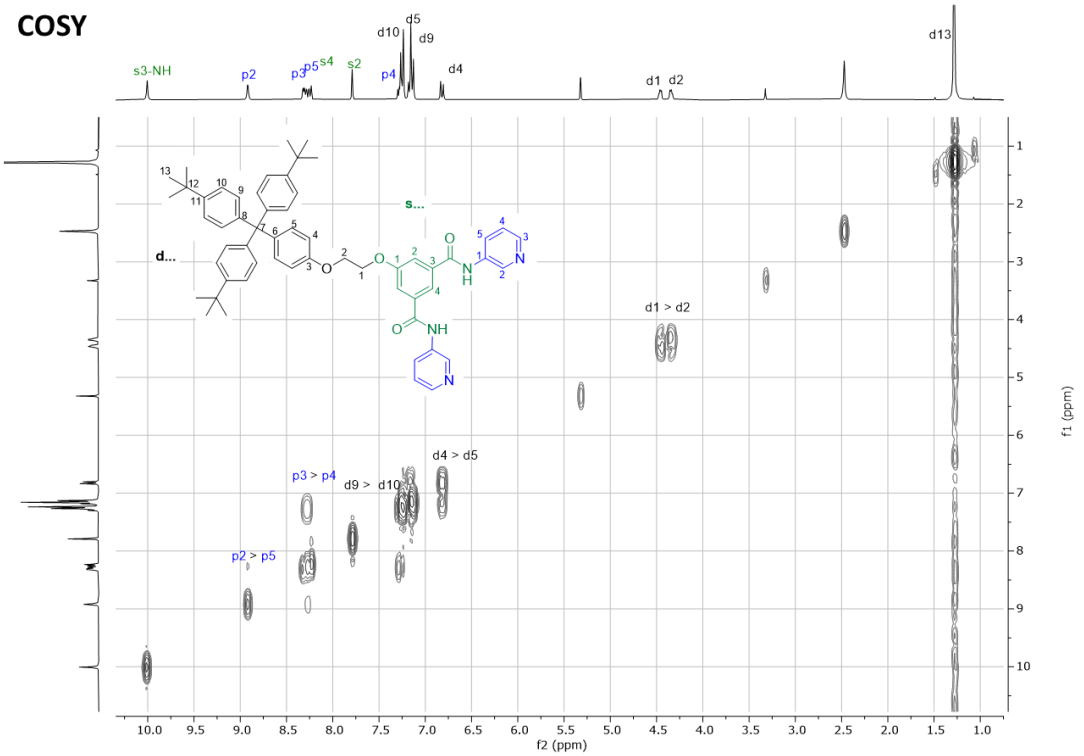

Figure S8. {^{1}H-^{1}H}-COSY NMR spectrum of dipyridyl ligand **1** in CD_2Cl_2 with 10% dmso-d_6, fully assigned.

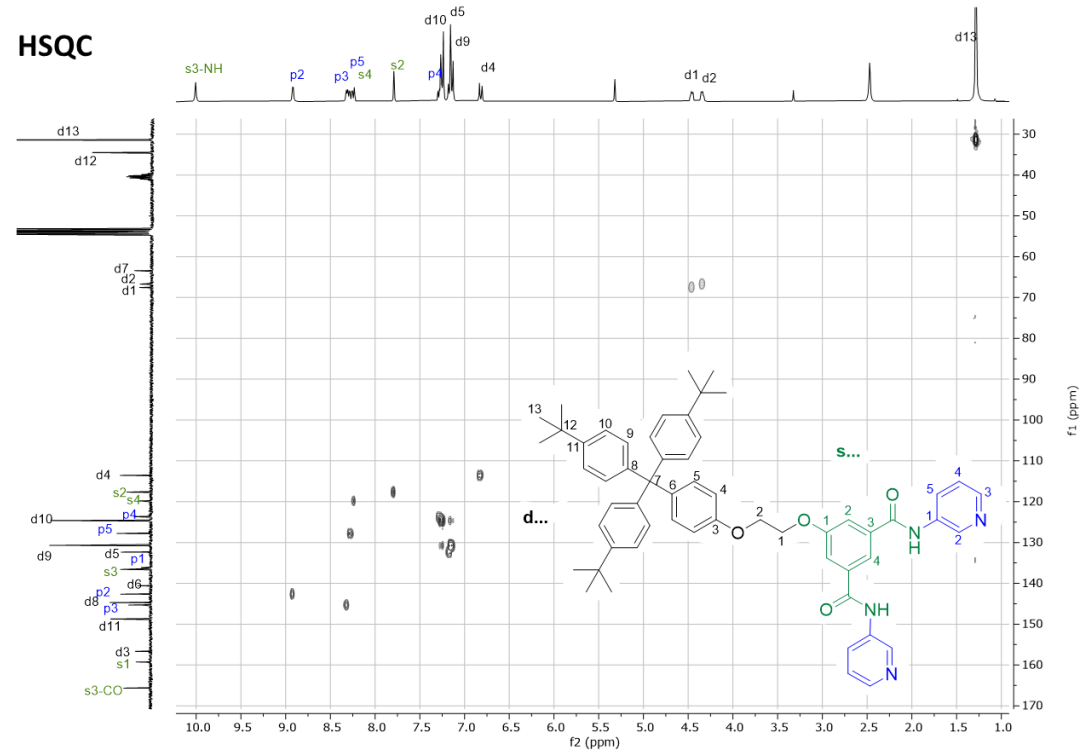

Figure S9. {^{1}H-^{13}C}-HSQC NMR spectrum of dipyridyl ligand **1** in CD_2Cl_2 with 10% dmso-d_6, fully assigned.

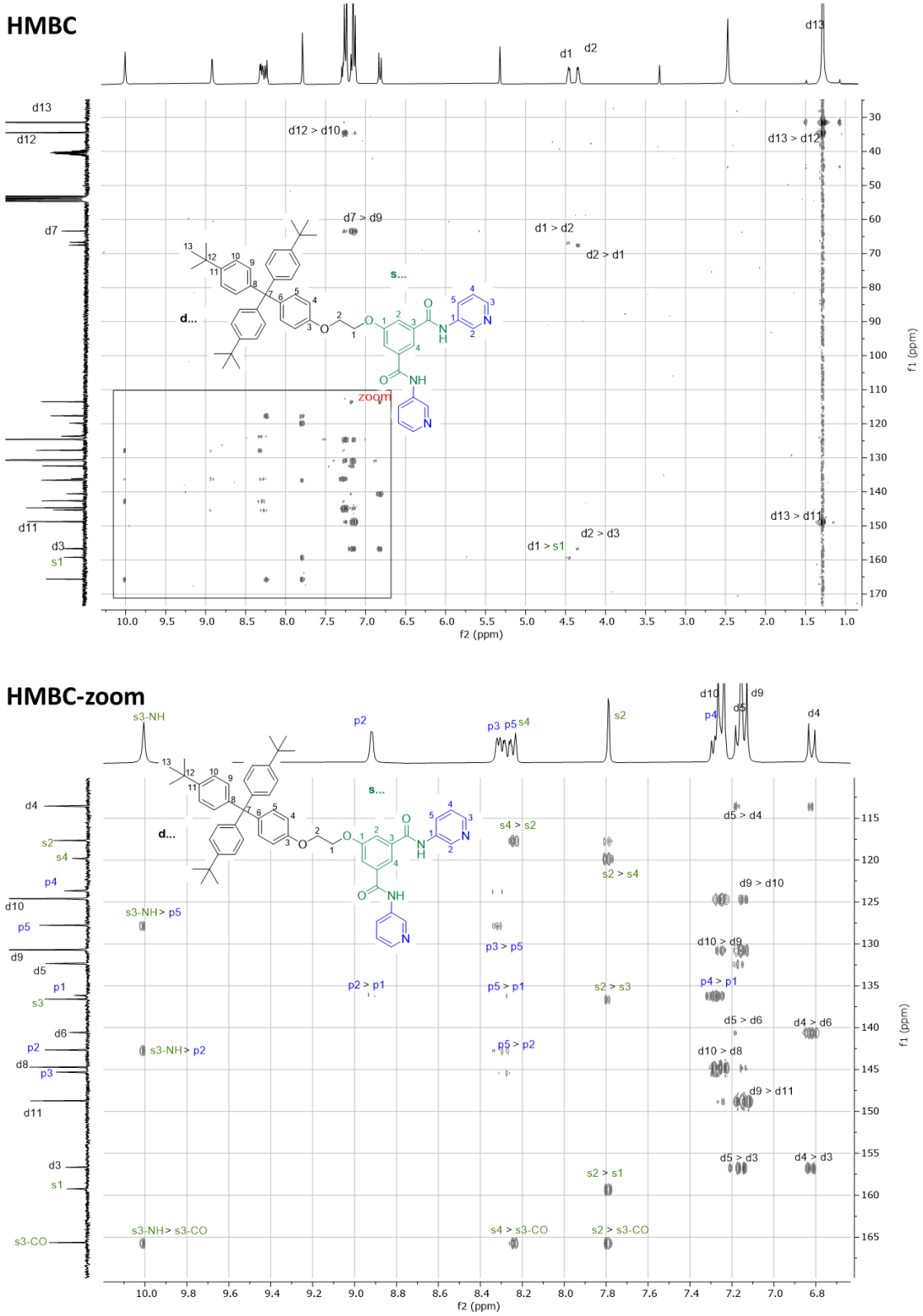

Figure S10. {^{1}H-^{13}C}-HMBC NMR spectrum of dipyridyl ligand **1** in CD_2Cl_2 with 10% dmso-d_6 with fully assigned zoom-in.

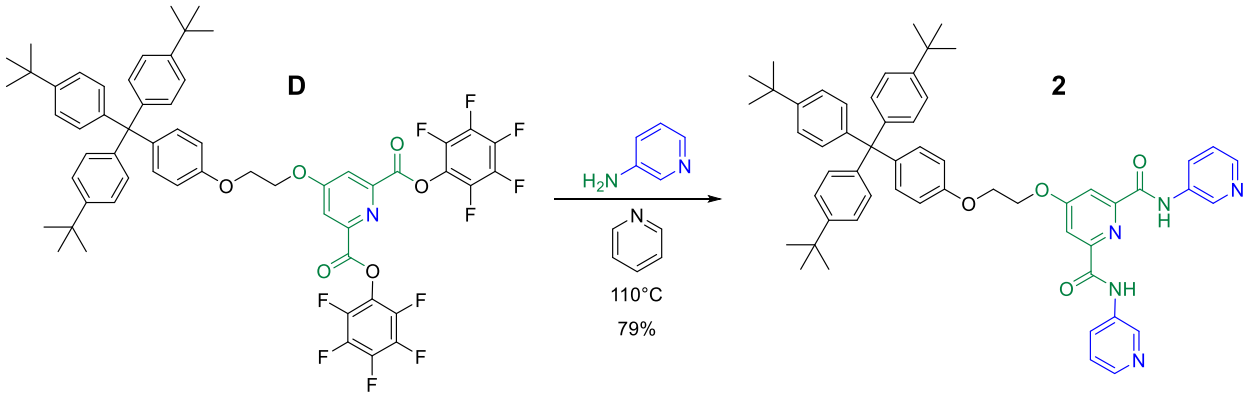

Dipyridyl ligand 2: Bis-pentafluorophenyl ester **D** (1.0 eq., 0.46 mmol, 481 mg), 3-aminopyridine (40 eq., 18.4 mmol, 1731 mg) and dry pyridine (5 mL) were mixed in a Schlenk flask. The mixture was heated to 110°C and stirred for 15h. After cooling to room temperature the product was precipitated by addition of H_2O (30 mL). The product was filtered, triturated with MeOH and filtered again. The residue was redissolved in CH_2Cl_2 (50 mL) dried over Na_2SO_4, filtered and concentrated *in vacuo*. The residue was further purified by flash column chromatography (2.5% MeOH in CH_2Cl_2 to 5% MeOH in CH_2Cl_2). Fractions containing the product were concentrated *in vacuo*. The residual solids were triturated with MeOH and filtered to afford dipyridyl ligand **2** (314 mg, 0.36 mmol, 79%) as white solid.

^{1}H NMR (500 MHz, 10% dmso-d_6 in CD_2Cl_2) δ 10.95 (s, 2H, s3-NH), 9.09 (s, 2H, p2), 8.53 – 8.21 (m, 4H, p5 and p3), 7.99 (s, 2H, s2), 7.32 (dd, J = 3.2 Hz, J = 4.6 Hz 2H, p4), 7.23 (d, J = 8.3 Hz, 6H, d10), 7.17 – 7.07 (m, 8H, d9 and d5), 6.80 (d, J = 8.6 Hz, 2H, d4), 4.55 (s, 2H, d1), 4.36 (s, 2H, d2), 1.26 (s, 27H, d13). **^{13}C NMR** (126 MHz, 10% dmso-d_6 in CD_2Cl_2) δ 168.04 (s3-CO), 162.49 (s1), 156.43 (d3), 151.17 (s3), 148.61 (d11), 145.61 (p3), 144.62 (d8), 143.22 (p2), 140.59 (d6), 135.30 (p1), 132.25 (d5), 130.62 (d9), 128.11 (p5), 124.53 (d10), 123.60 (p4), 113.56 (d4), 112.06 (s2), 67.94 (d1), 66.32 (d2), 63.32 (d7), 34.42 (d12), 31.34 (d13). **MS** (MS FD+ eiFi, m/z) calc. for $C_{56}H_{59}N_5O_4$ $[M]^+$: 865.4567, found: 865.4585.

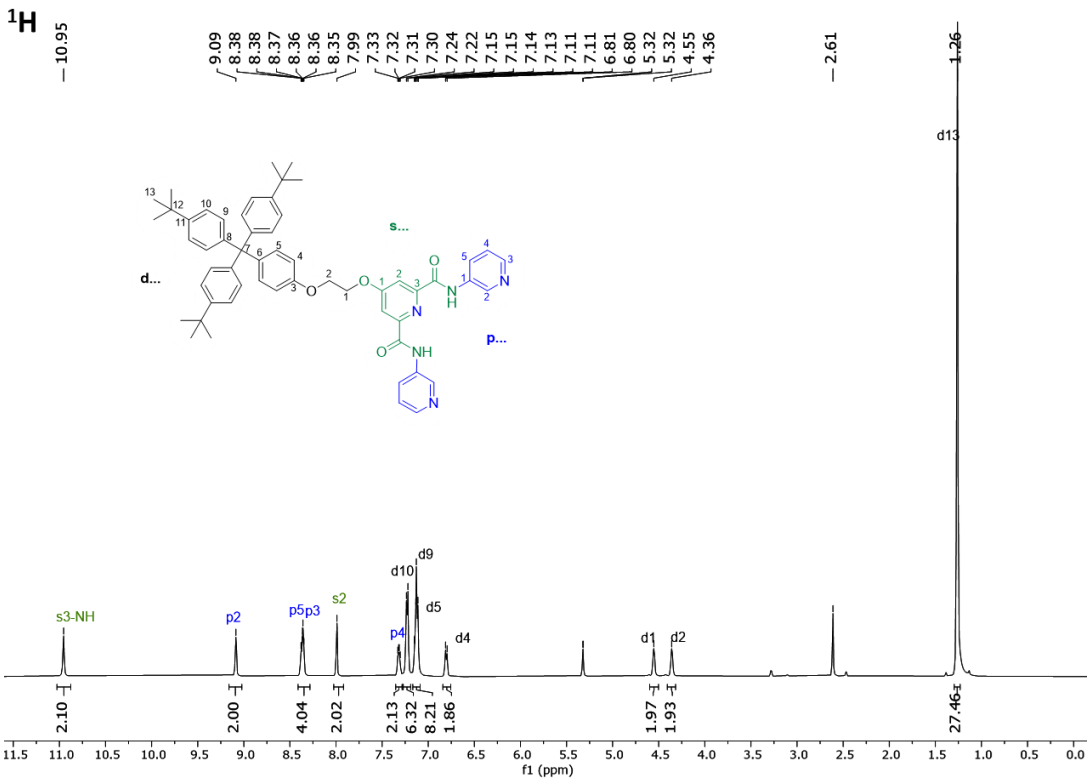

Figure S11. ^{1}H NMR spectrum of dipyridyl ligand **2** in CD_2Cl_2 with 10% dmso-d_6, fully assigned.

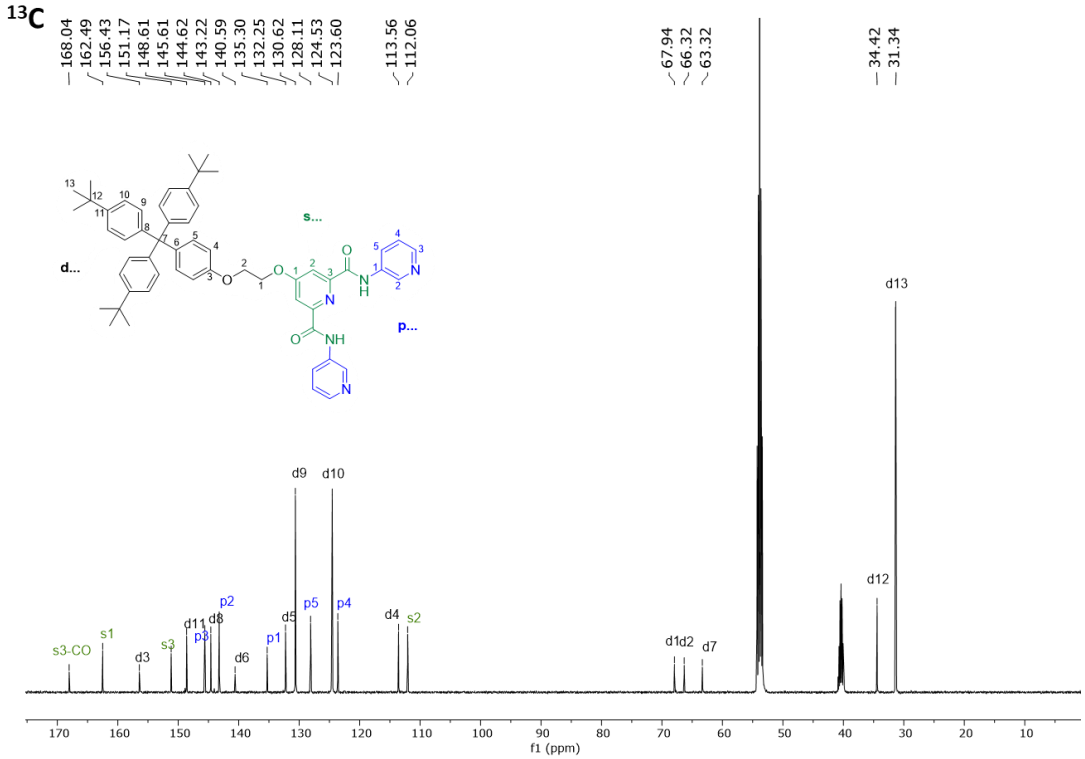

Figure S12. ^{13}C NMR spectrum of ligand **2** in CD_2Cl_2 with 10% dmso-d_6, fully assigned.

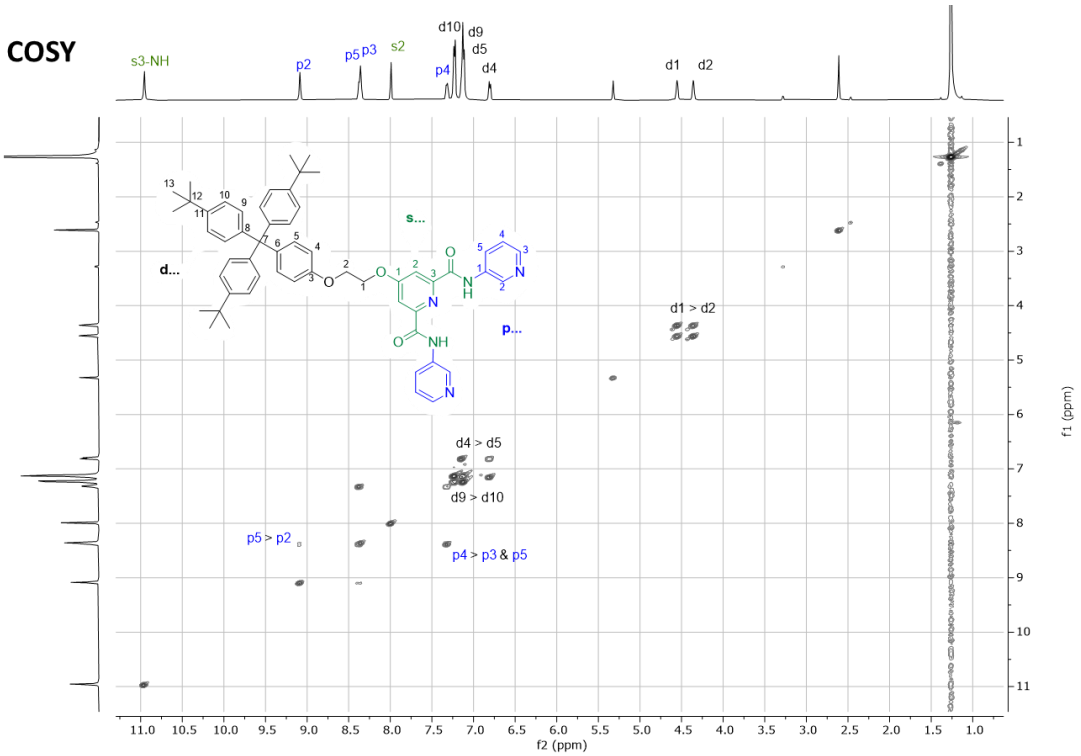

Figure S13. {^{1}H-^{1}H}-COSY NMR spectrum of dipyridyl ligand **2** in CD_2Cl_2 with 10% dmso-d_6, fully assigned.

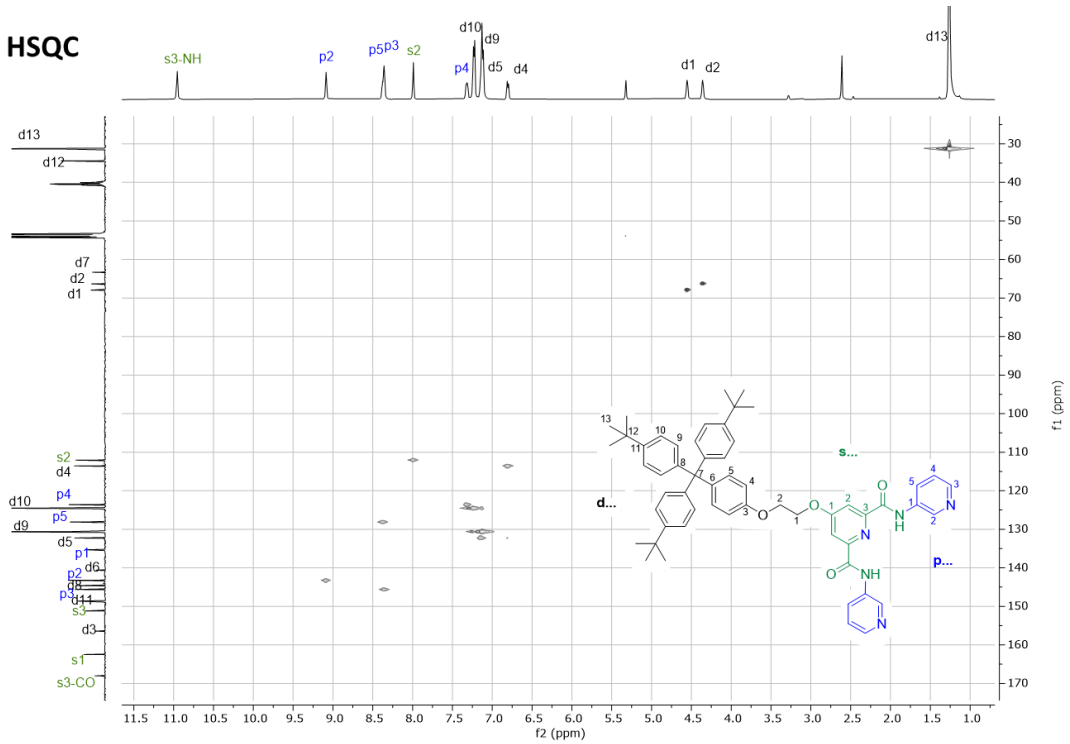

Figure S14. {^{1}H-^{13}C}-HSQC NMR spectrum of dipyridyl ligand **2** in CD_2Cl_2 with 10% dmso-d_6, fully assigned.

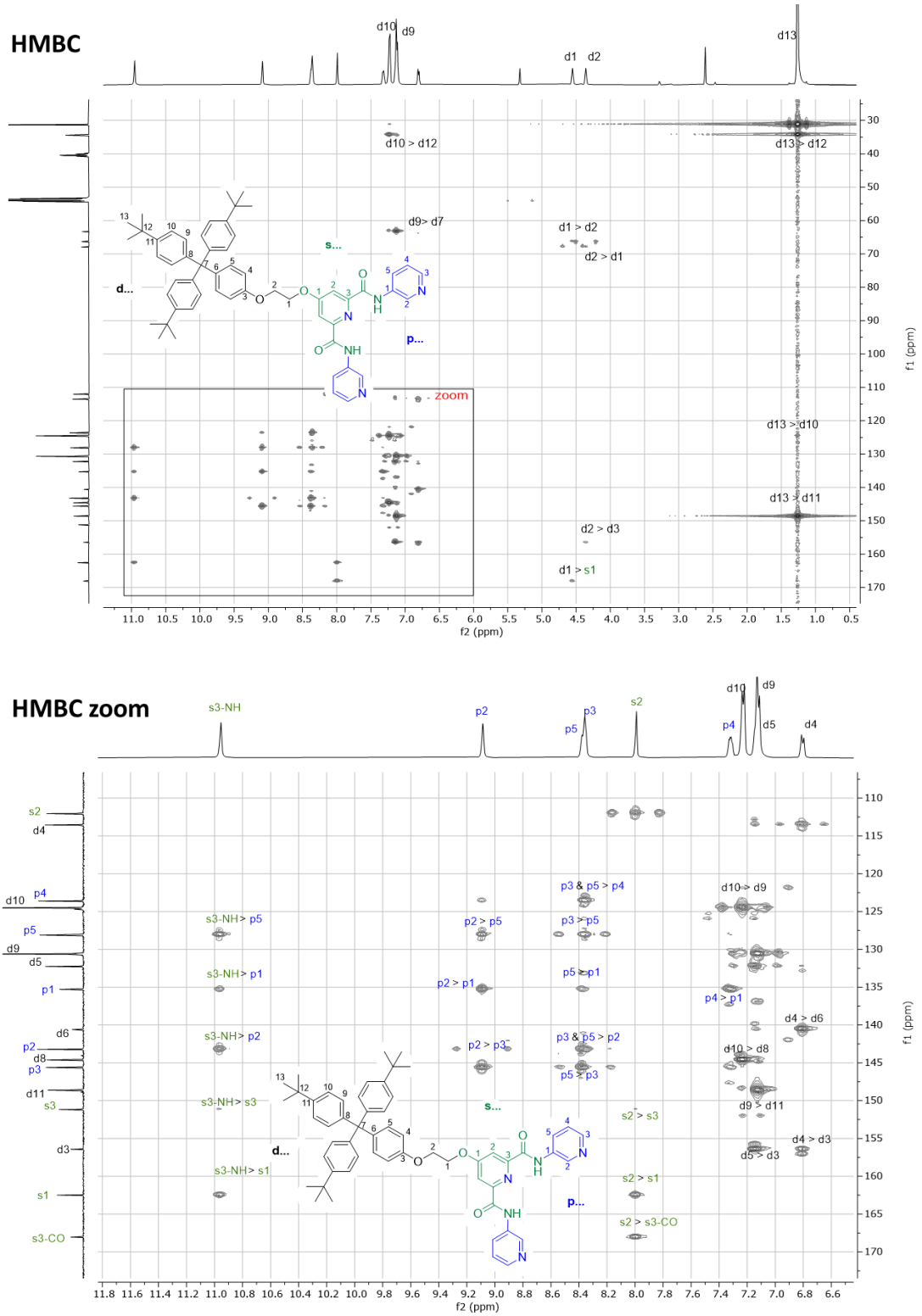

Figure S15. {^{1}H-^{13}C}-HMBC NMR spectrum of dipyridyl ligand **2** in CD_2Cl_2 with 10% dmso-d_6 with fully assigned zoom-in.

Section S2c. Synthesis and characterizations of Pd complexes

Cages $[Pd_21_4][BF_4]_4$ and $[Pd_22_4][BF_4]_4$: The M_2L_4 cages were prepared by slow addition of the $[Pd(CH_3CN)_4][BF_4]_2$ precursor in dmso-d_6 to a solution of the desired ligand (**1** or **2**) in CH_2Cl_2 with the remainder of dmso-d_6 to end up at 5 *v/v*% of dmso-d_6. Initially, multiple products are formed which converge to the thermodynamic M_2L_4 cages by stirring for approximately 1 week. See also **Figure S36** and **Figure S37** for the formation studies.

$[Pd_21_4][BF_4]_4$ (Figure S16– Figure S23 and Figure S33)

^{1}H NMR (500 MHz, 5% dmso-d_6 in CD_2Cl_2) δ 10.21 (s, 8H, s3-NH), 9.85 (s, 8H, p2), 9.10 (d, *J* = 4.5 Hz, 8H, p3), 8.62 (d, *J* = 6.8 Hz, 8H, p5), 8.44 (s, 4H, s4), 7.85 (s, 8H, s2), 7.50 (dd, *J* = 8.5, 5.8 Hz, 8H, p4), 7.22 (d, *J* = 8.6 Hz, 24H, d10), 7.13 – 7.09 (t, *J* = 9.6 Hz, 32H, d5 and d9), 6.75 (d, *J* = 9.0 Hz, 8H, d4), 4.39 (s, 8H, d1), 4.27 (s, 8H, d2), 1.26 (s, 108H, d13).**^{13}C NMR** (126 MHz, 5% dmso-d_6 in CD_2Cl_2) δ 165.39 (s3-CO), 159.50 (s1), 156.56 (d3), 148.75 (d11), 146.53 (p3), 144.67 (d8), 142.34 (p2), 140.61 (d6), 139.11 (p1), 135.27 (s3), 132.34 (d5), 131.34 (p5), 130.67 (d9), 127.36 (p4), 124.60 (d10), 119.25 (s4), 118.59 (s2), 113.44 (d4), 67.66 (d1), 66.56 (d2), 63.38 (d7), 34.49 (d12), 31.39 (d13). **^{19}F NMR** (282 MHz, 5% dmso-d_6 in CD_2Cl_2) δ -148.52. **CSI HRMS**: m/z calculated for $[Pd_2(C_{57}H_{60}N_4O_4)_4]^{4+}$ = 918.1650, found 918.1582; $\{[Pd_2(C_{57}H_{60}N_4O_4)_4][BF_4]\}^{3+}$ = 1253.2214, found 1253.2121; $\{[Pd_2(C_{57}H_{60}N_4O_4)_4][BF_4]_2\}^{2+}$ = 1923.3342, found 1923.3190.

$[Pd_22_4][BF_4]_4$ (Figure S24 – Figure S33)

^{1}H NMR (500 MHz, 5% dmso-d_6 in CD_2Cl_2) δ 10.49 (s, 8H, s3-NH), 9.09 (d, *J* = 9.0 Hz, 8H, p5), 8.90 (s, 8H, p2), 8.73 (d, *J* = 5.8 Hz, 8H, p3), 7.95 (s, 8H, s2), 7.53 (dd, *J* = 8.6, 5.8 Hz, 8H, p4), 7.22 (d, *J* = 8.5 Hz, 24H, d10), 7.13 – 7.10 (m, 32H, d9 and d5), 6.76 (d, *J* = 8.9 Hz, 8H, d4), 4.47 (s, 8H, d1), 4.30 (s, 8H, d2), 1.26 (s, 108H, d13). **^{13}C NMR** (126 MHz, CD_2Cl_2) δ 168.09 (s3-CO), 163.06 (s1), 156.39 (d3), 150.54 (s3), 148.73 (d11), 147.00 (p3), 144.66 (d8), 143.70 (p2), 140.86 (d6), 138.16 (p1), 132.50 (p5), 132.33 (d5), 130.68 (d9), 127.23 (p4), 124.60 (d10), 113.54 (s2), 113.27 (d4), 68.05 (d1), 66.61 (d2), 63.92 (d7), 34.49 (d12), 31.39 (d13). **^{19}F NMR** (282 MHz, 5% dmso-d_6 in CD_2Cl_2) δ -148.13. **CSI HRMS**: m/z calculated for $[Pd_2(C_{56}H_{59}N_5O_4)_4]^{4+}$ = 919.1602, found 919.1588; $\{[Pd_2(C_{56}H_{59}N_5O_4)_4][BF_4]\}^{3+}$ = 1254.5483, found 1254.5385; $\{[Pd_2(C_{56}H_{59}N_5O_4)_4][BF_4]_2\}^{2+}$ = 1925.3246, found 1925.3095.

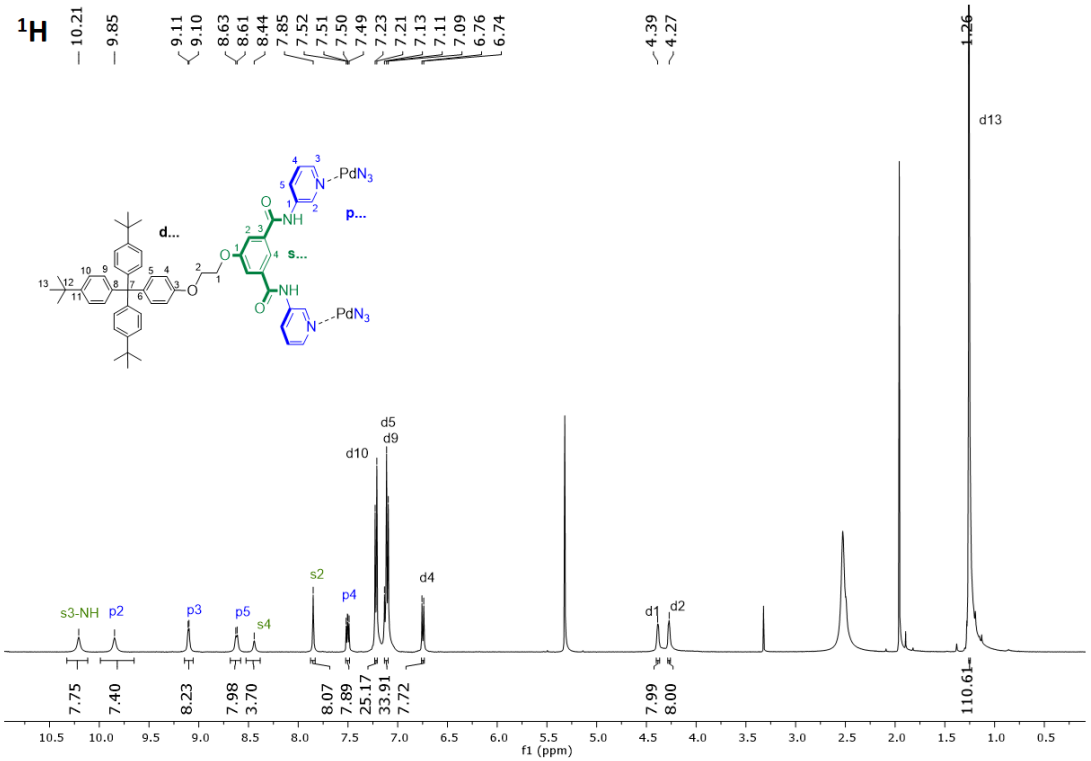

Figure S16. ^{1}H NMR spectrum of $[Pd_2\mathbf{1}_4][BF_4]_4$ in CD_2Cl_2 with 5% dmso-d_6, fully assigned.

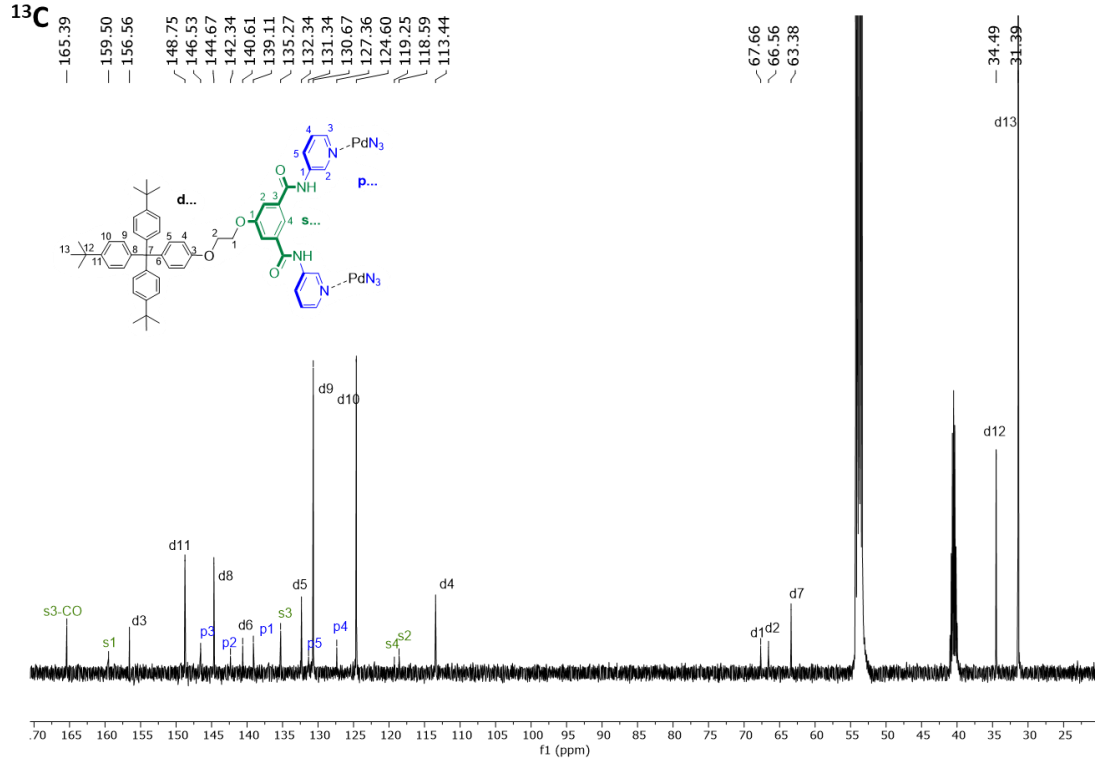

Figure S17. ^{13}C NMR spectrum of $[Pd_2\mathbf{1}_4][BF_4]_4$ in CD_2Cl_2 with 5% dmso-d_6, fully assigned.

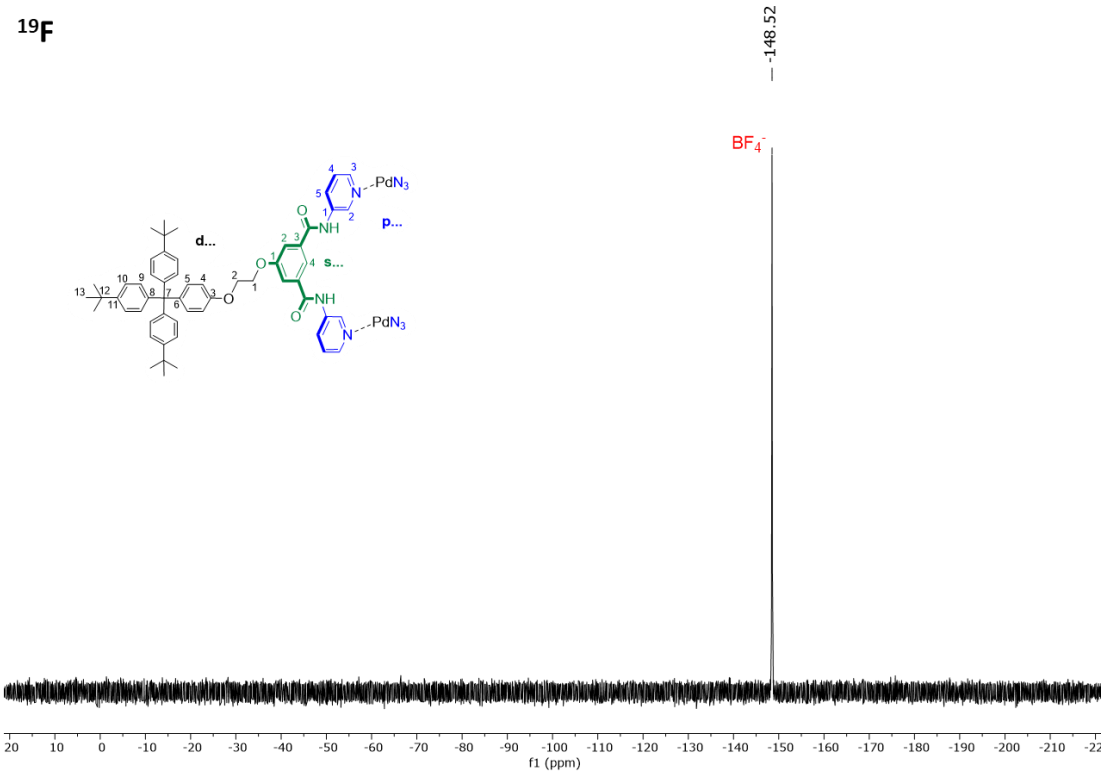

Figure S18. ^{19}F NMR spectrum of $[Pd_2\mathbf{1}_4][BF_4]_4$ in CD_2Cl_2 with 5% dmso-d_6, fully assigned.

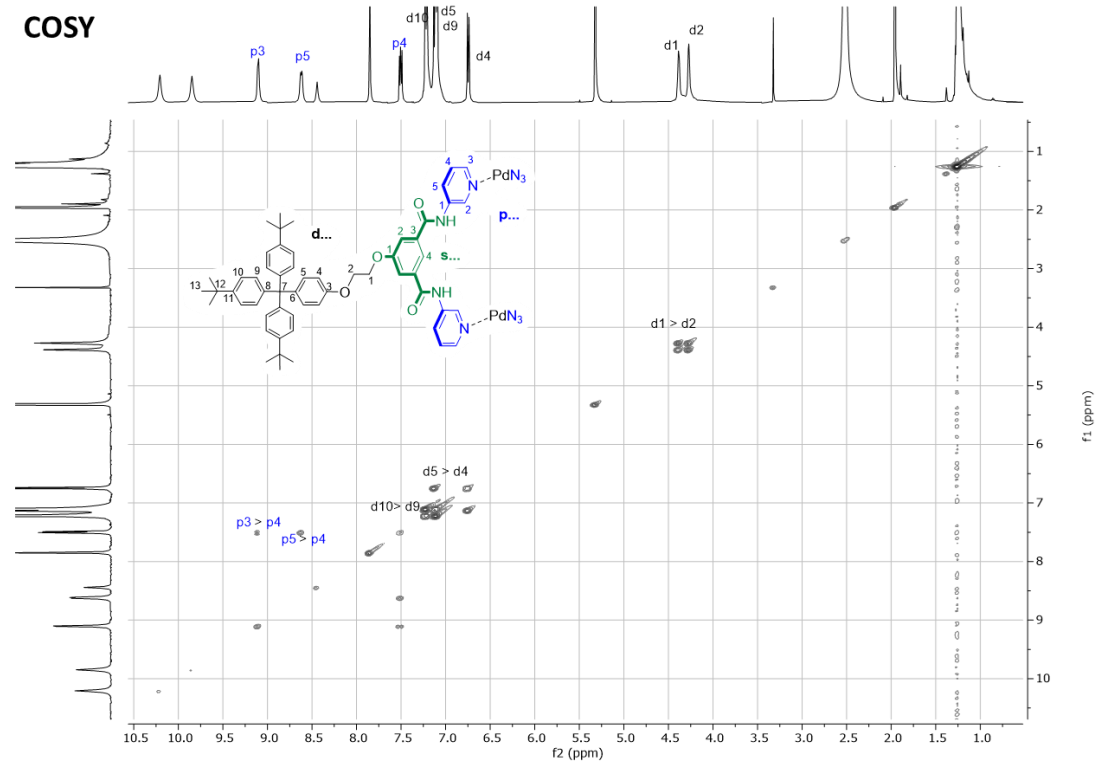

Figure S19. {^1H-^1H}-COSY NMR spectrum of $[Pd_2\mathbf{1}_4][BF_4]_4$ in CD_2Cl_2 with 5% dmso-d_6, fully assigned.

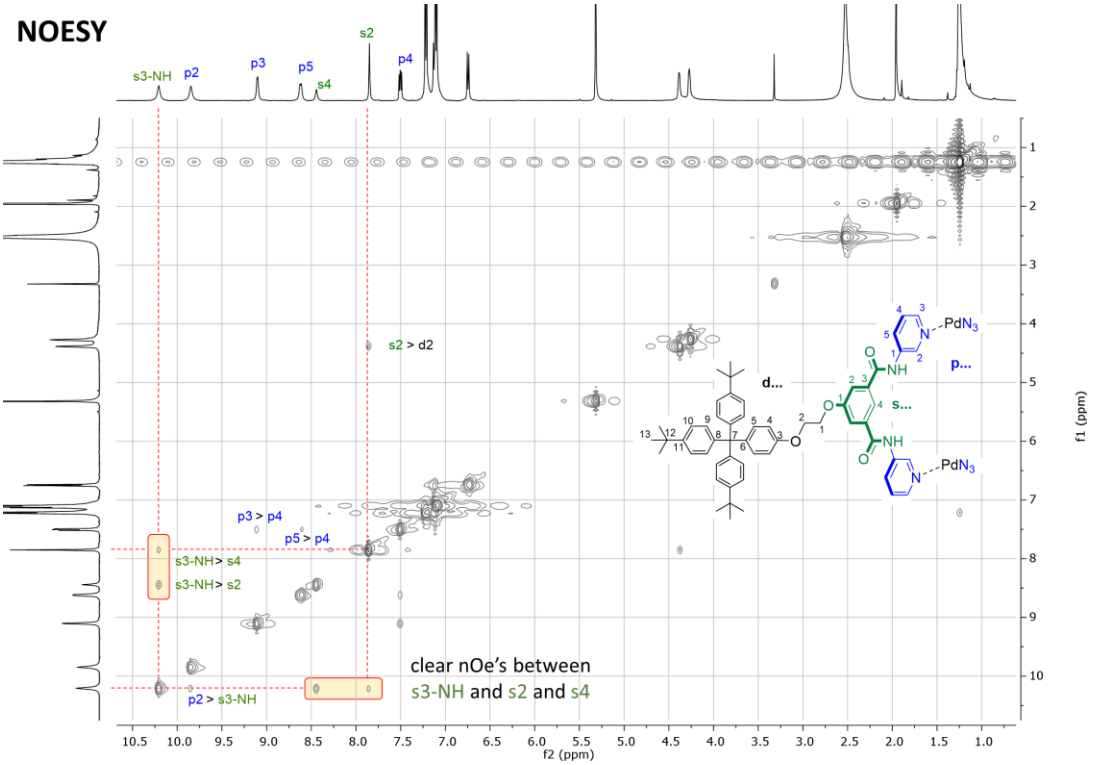

Figure S20. {^{1}H-^{1}H}-NOESY NMR spectrum of $[Pd_2\mathbf{1}_4][BF_4]_4$ in CD_2Cl_2 with 5% dmso-d_6, fully assigned. **NB:** note the clear nOe contacts between **s3-NH** and both **s4** and **s2** highlighted in the spectrum.

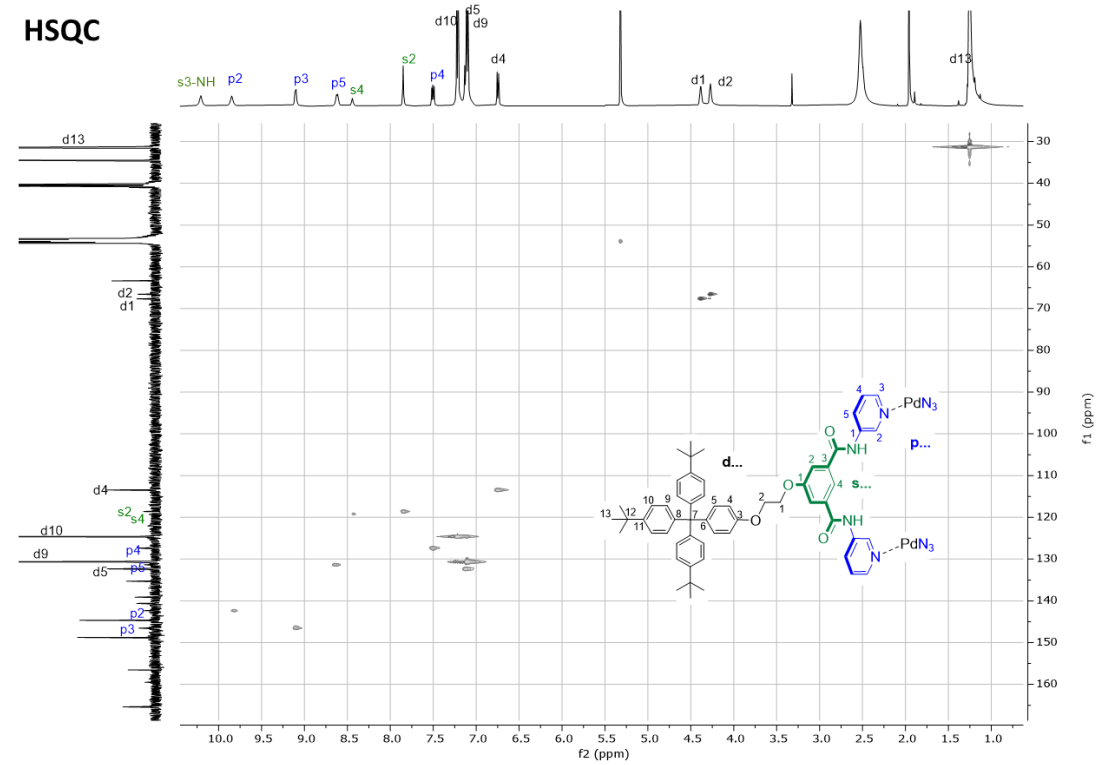

Figure S21. {^{1}H-^{13}C}-HSQC NMR spectrum of $[Pd_2\mathbf{1}_4][BF_4]_4$ in CD_2Cl_2 with 5% dmso-d_6, fully assigned.

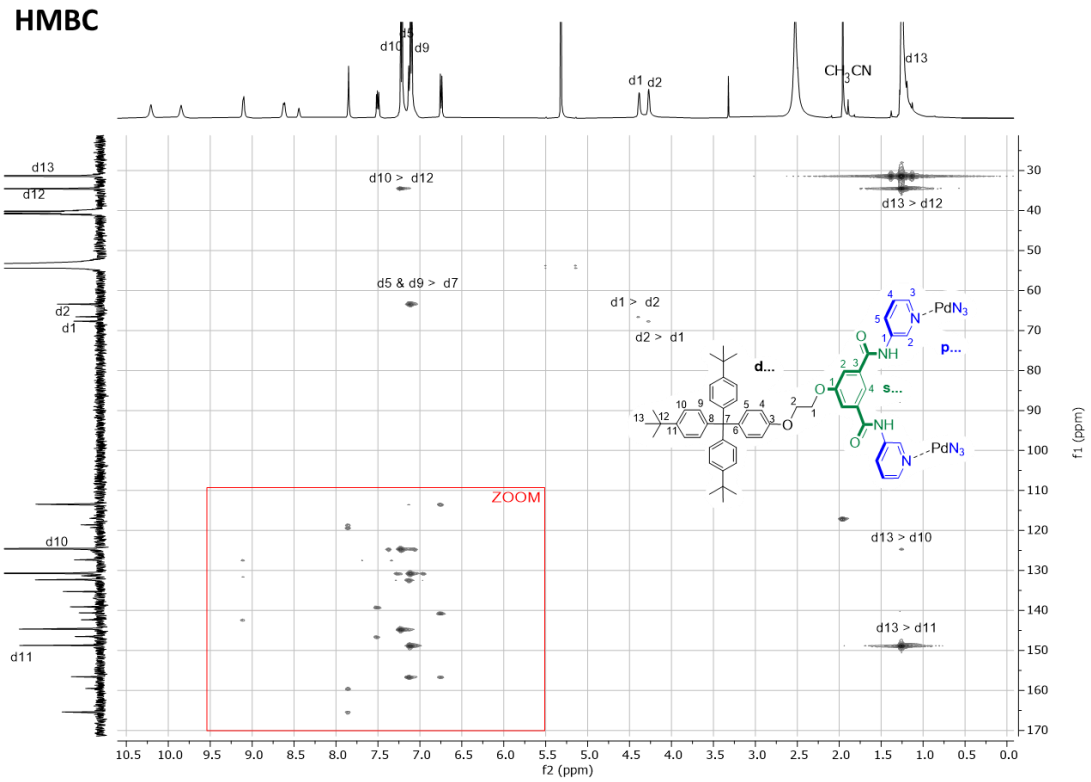

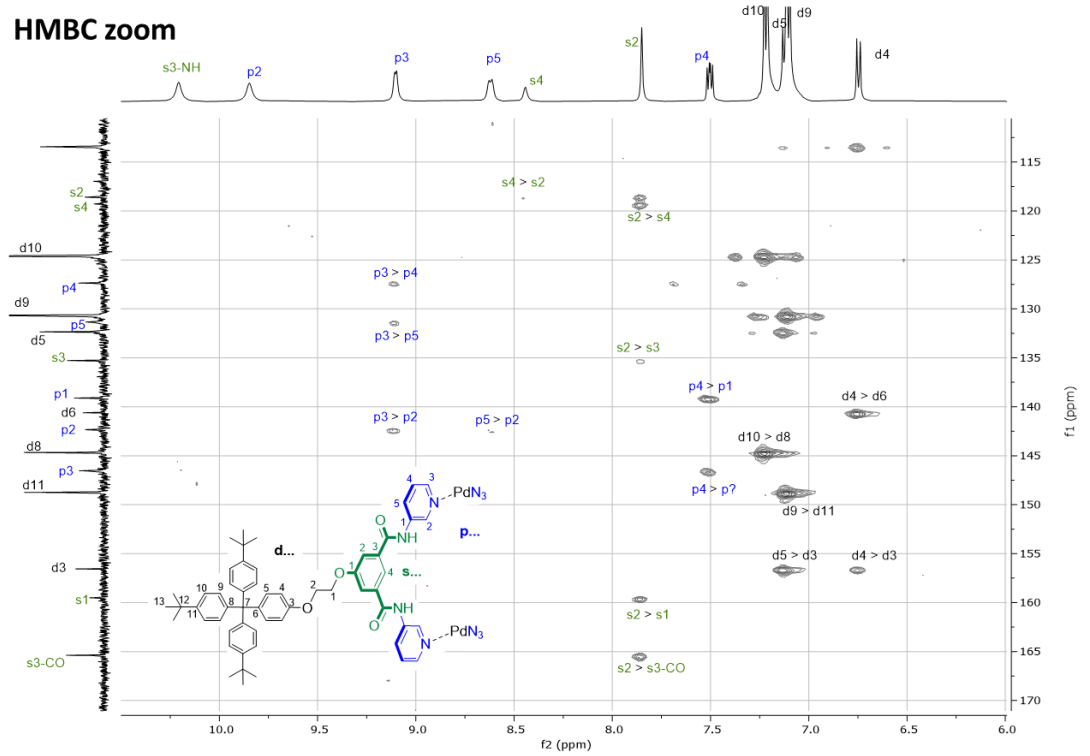

Figure S22. {^{1}H-^{13}C}-HMBC NMR spectrum of $[Pd_2\mathbf{1}_4][BF_4]_4$ in CD_2Cl_2 with 5% dmso-d_6 with fully assigned zoom-in.

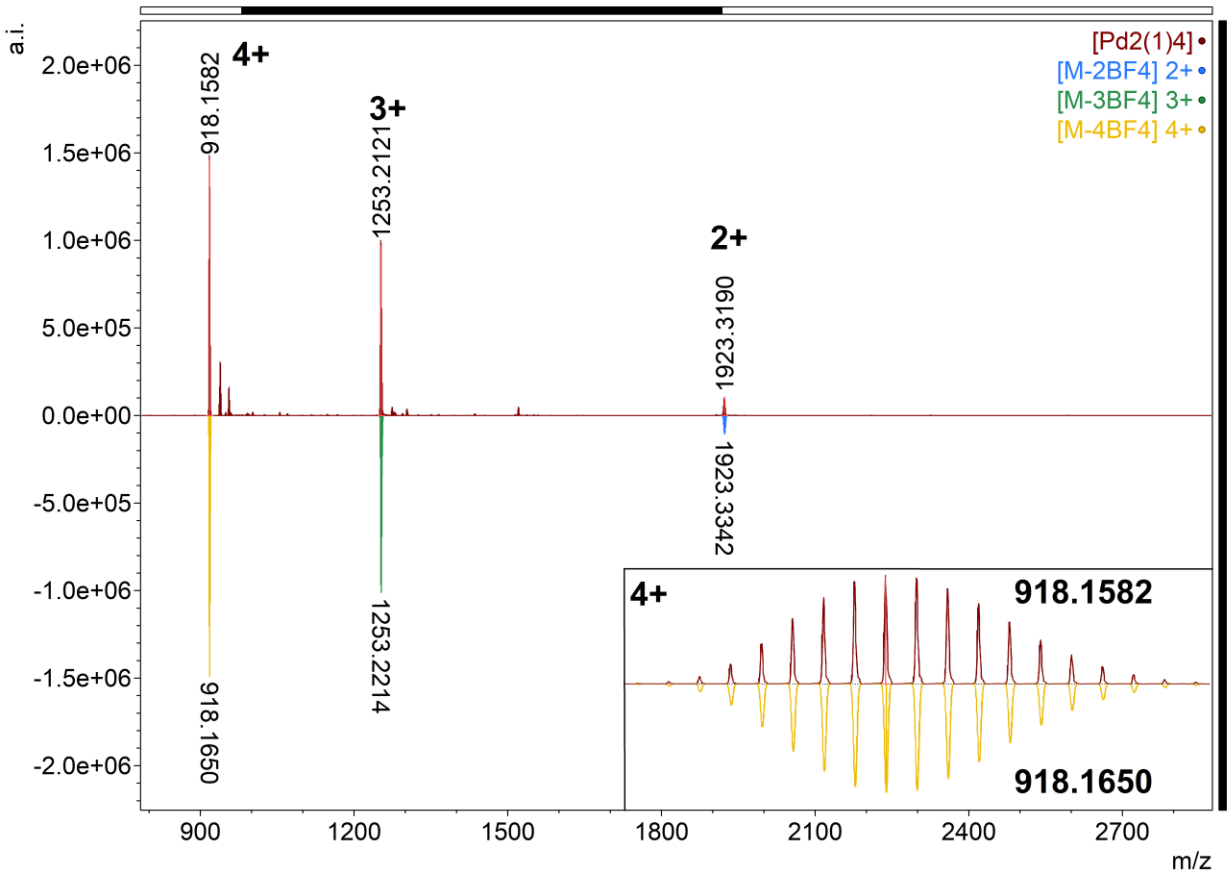

Figure S23. ESI-MS spectrum of $[Pd_2\mathbf{1}_4]^{4+}$ and its BF_4^- adducts as measured (top) and simulated (bottom). The inset figure shows the measured and simulated monoisotopic mass distribution of the largest peak, $[Pd_2\mathbf{1}_4]^{4+}$.

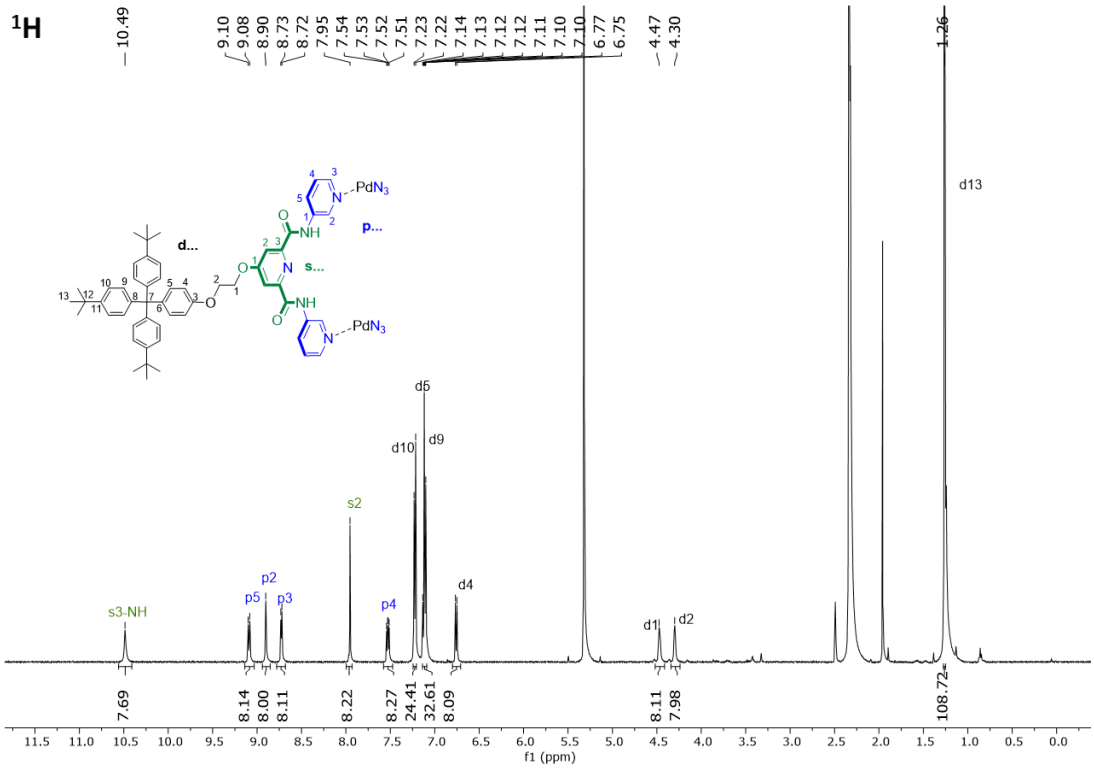

Figure S24. ^{1}H NMR spectrum of $[Pd_2\mathbf{2}_4][BF_4]_4$ in CD_2Cl_2 with 5% dmso-d_6, fully assigned.

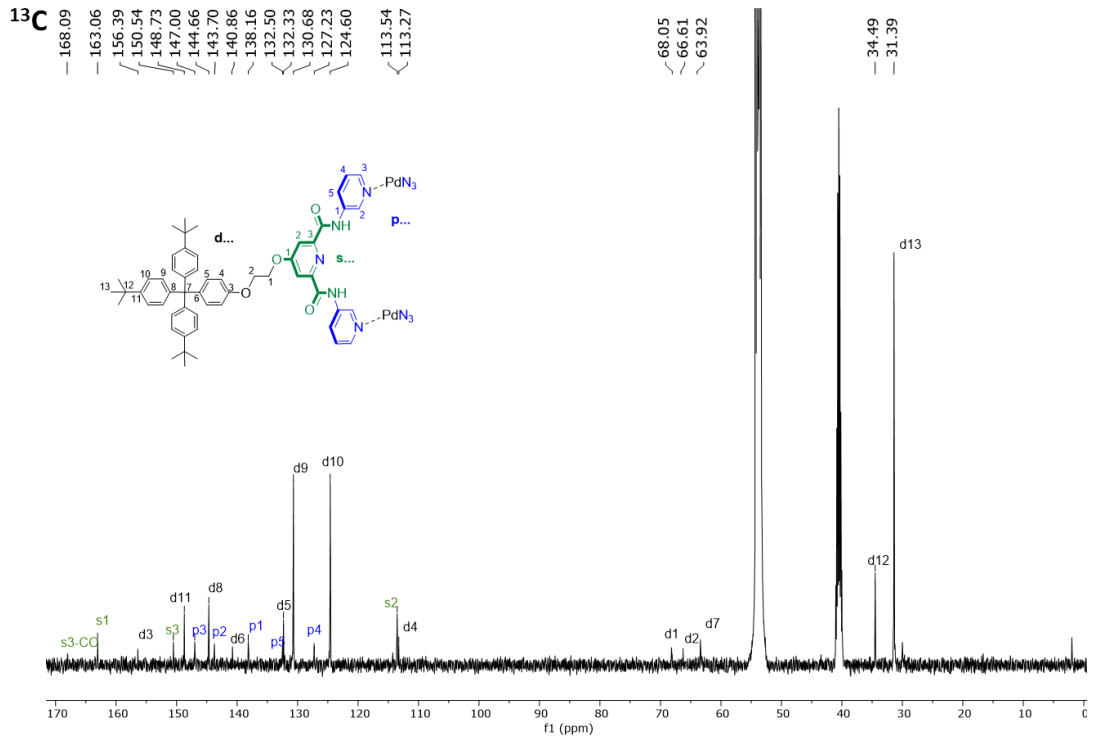

Figure S25. ^{13}C NMR spectrum of $[Pd_2\mathbf{2}_4][BF_4]_4$ in CD_2Cl_2 with 5% dmso-d_6, fully assigned.

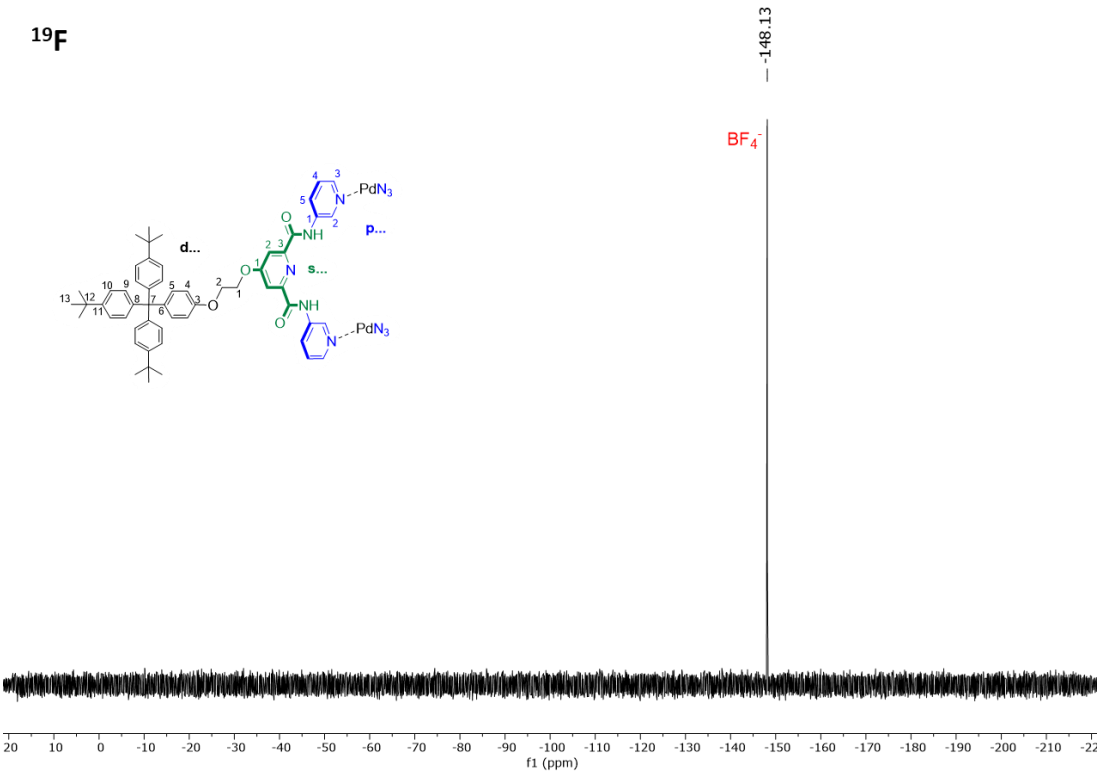

Figure S26. ^{19}F NMR spectrum of $[Pd_2\mathbf{2}_4][BF_4]_4$ in CD_2Cl_2 with 5% dmso-d_6, fully assigned.

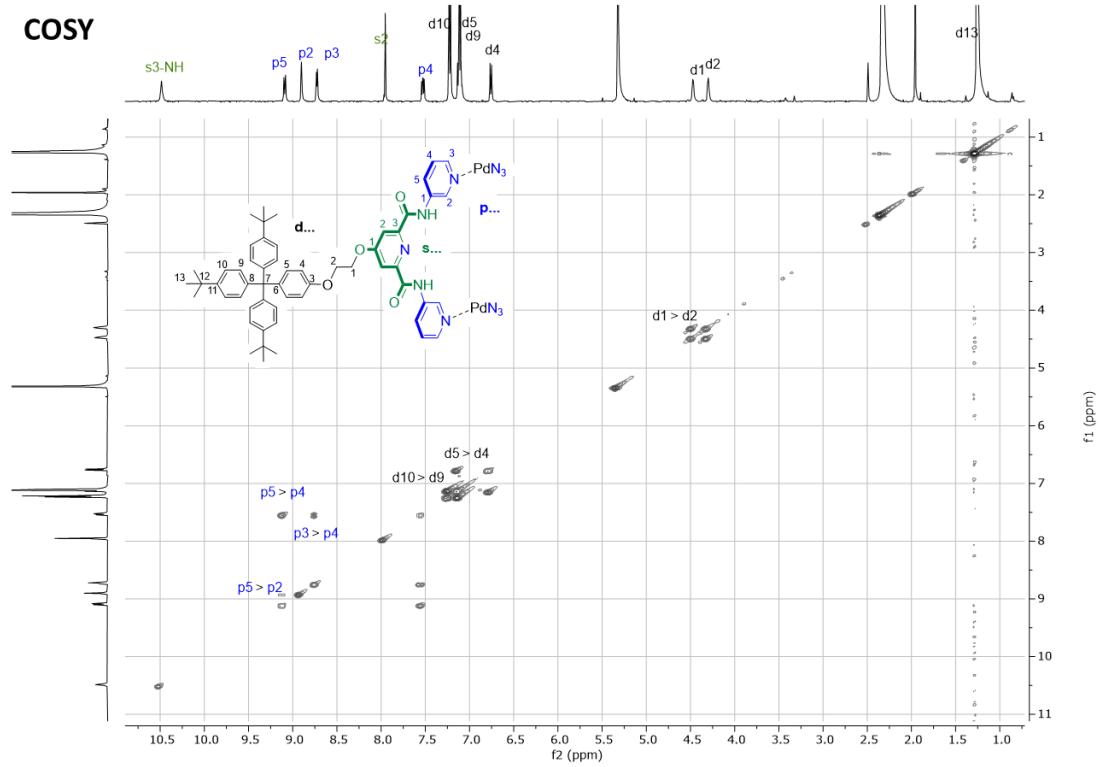

Figure S27. {^{1}H-^{1}H}-COSY NMR spectrum of $[Pd_2\mathbf{2}_4][BF_4]_4$ in CD_2Cl_2 with 5% dmso-d_6, fully assigned.

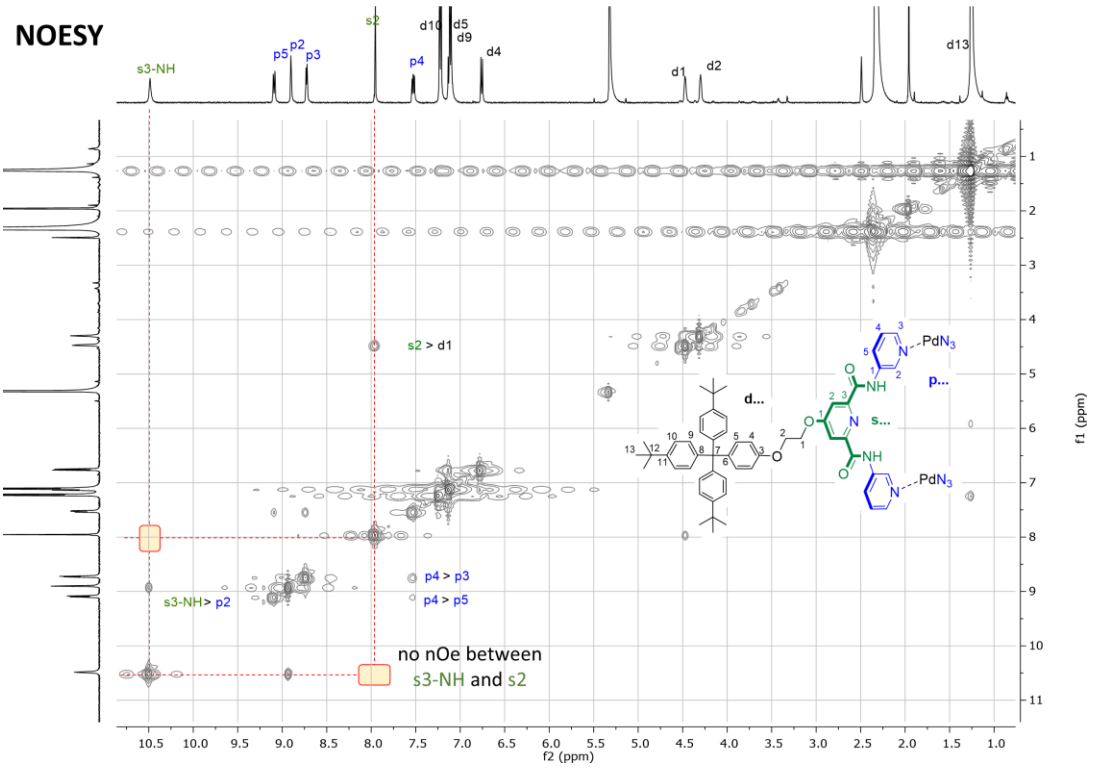

Figure S28. {^{1}H-^{1}H}-NOESY NMR spectrum of $[Pd_2\mathbf{2}_4][BF_4]_4$ in CD_2Cl_2 with 5% dmso-d_6, fully assigned. **NB:** note the absence of a nOe contact between **s2** and **s3-NH** highlighted in the spectrum.

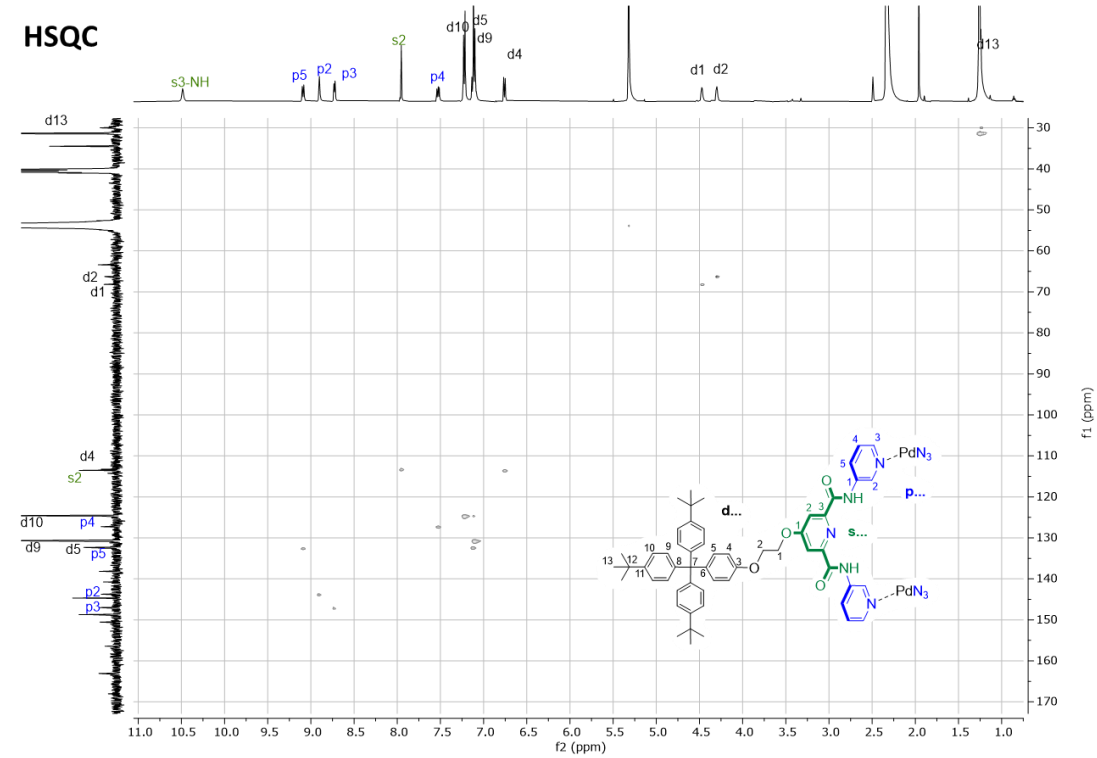

Figure S29. {^{1}H-^{13}C}-HSQC NMR spectrum of $[Pd_2\mathbf{2}_4][BF_4]_4$ in CD_2Cl_2 with 5% dmso-d_6, fully assigned.

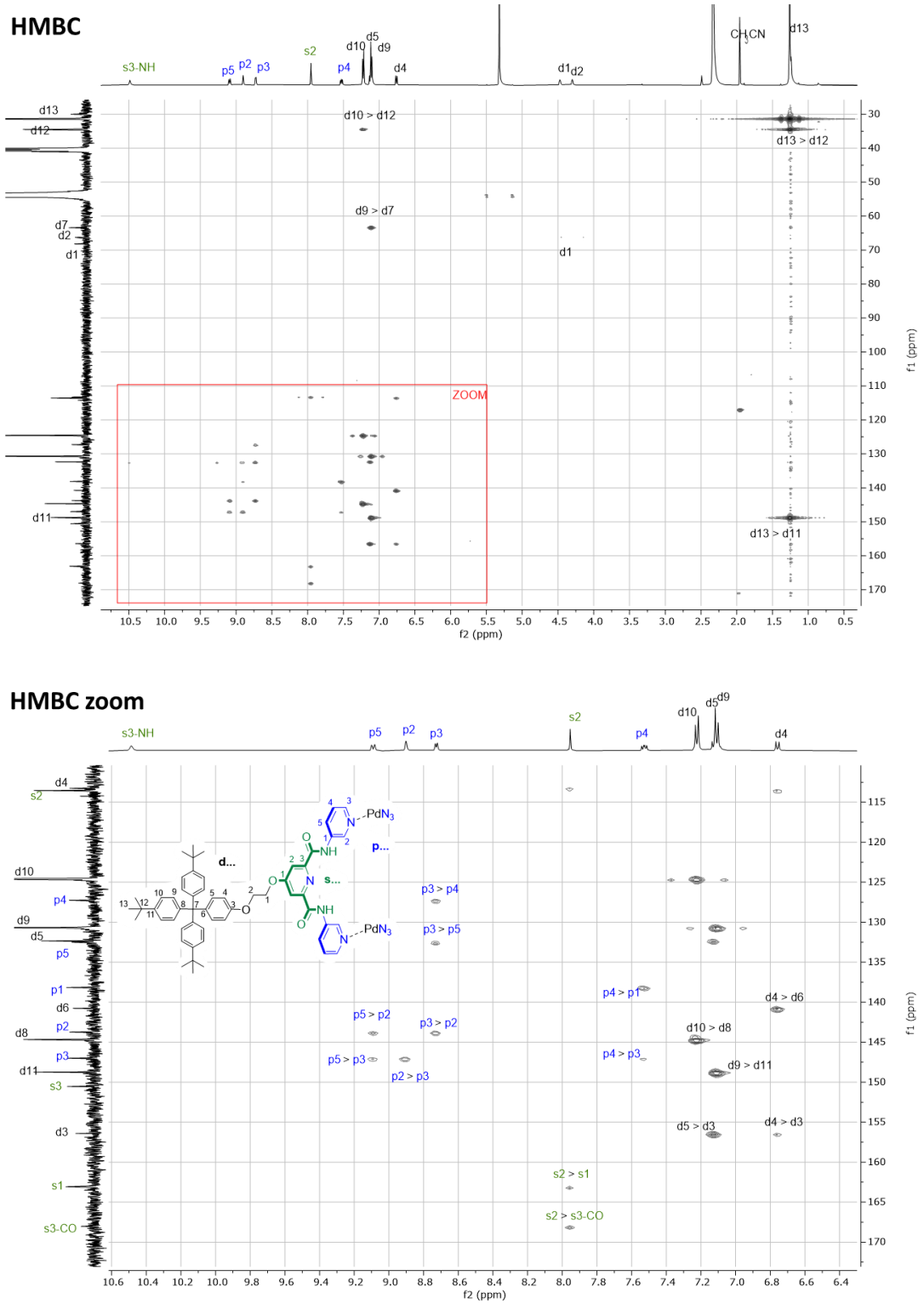

Figure S30. {^{1}H-^{13}C}-HMBC NMR spectrum of $[Pd_2\mathbf{2}_4][BF_4]_4$ in CD_2Cl_2 with 5% dmso-d_6 with fully assigned zoom-in.

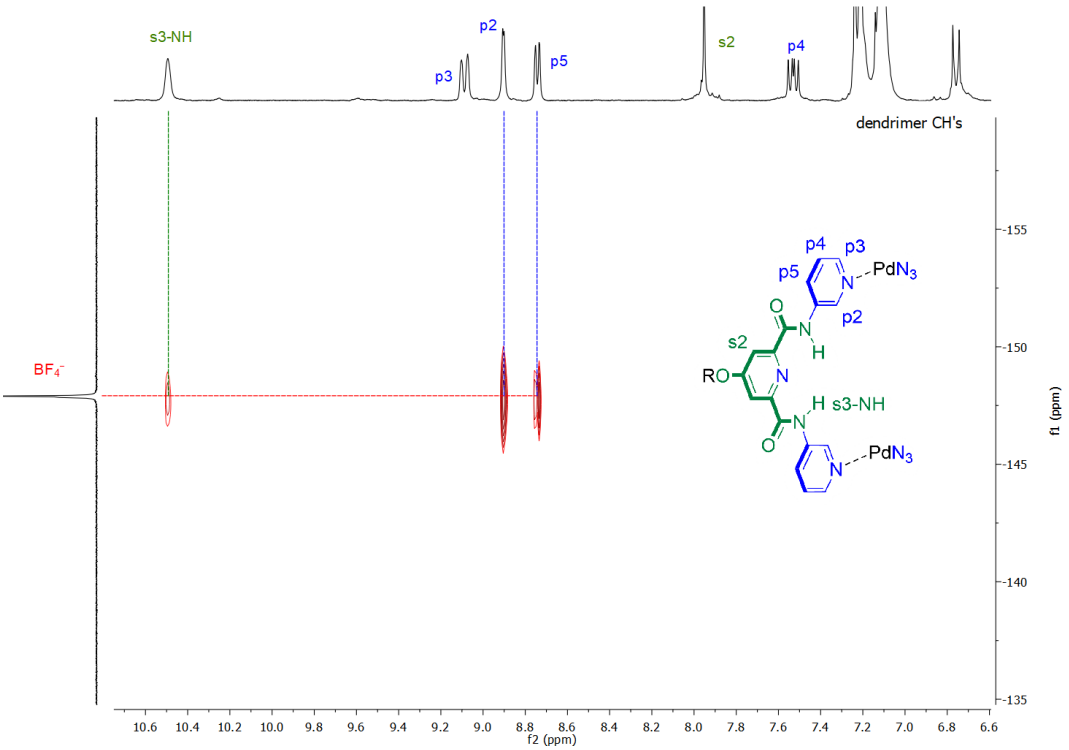

Figure S31. {^{1}H-^{19}F}-HOESY NMR spectrum of $[Pd_2\mathbf{2}_4][BF_4]_4$ in CD_2Cl_2 with 5% dmso-d_6, fully assigned. The nOe's between BF_4^- and **s3-NH** and **p2** evidences that the anion is predominantly bound to the interior of $[Pd_2\mathbf{2}_4][BF_4]_4$. The nOe to **p5** further evidence anion binding to the exterior of the cage.

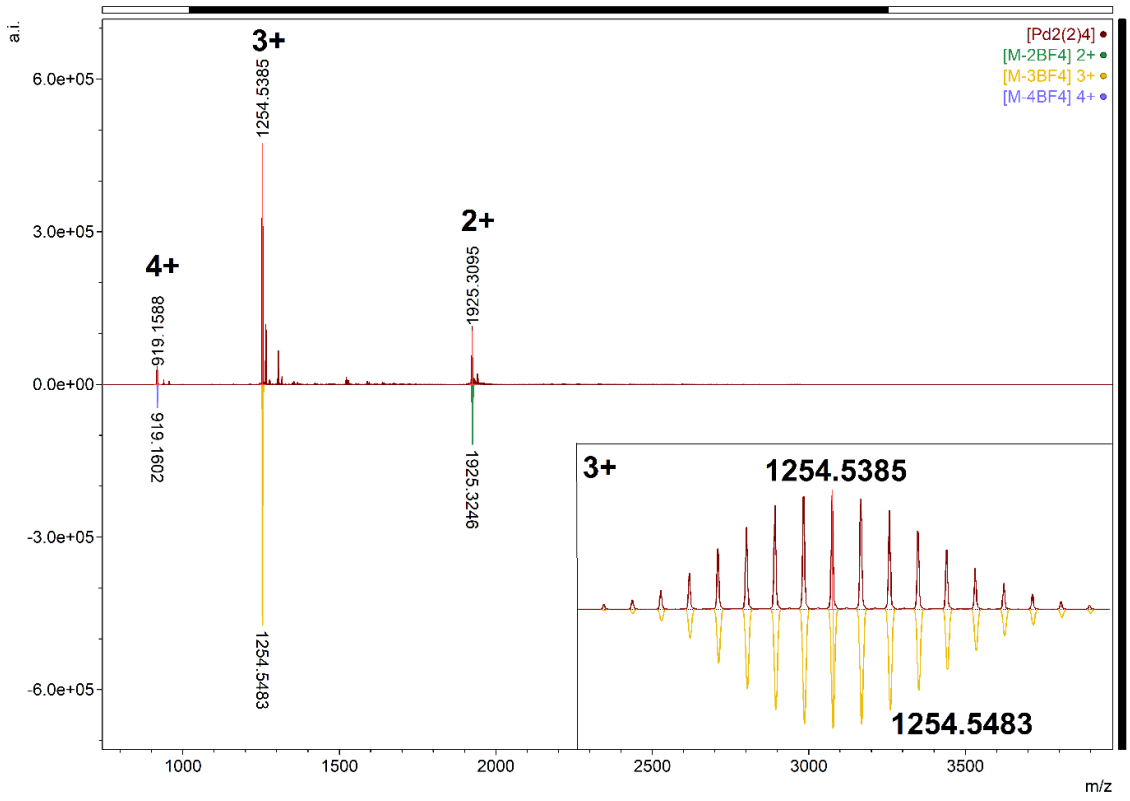

Figure S32. ESI-MS spectrum of $[Pd_2\mathbf{2}_4]^{4+}$ and its BF_4^- adducts as measured (top) and simulated (bottom). The inset figure shows the measured and simulated monoisotopic mass distribution of the largest peak, $\{[Pd_2\mathbf{2}_4][BF_4]\}^{3+}$.

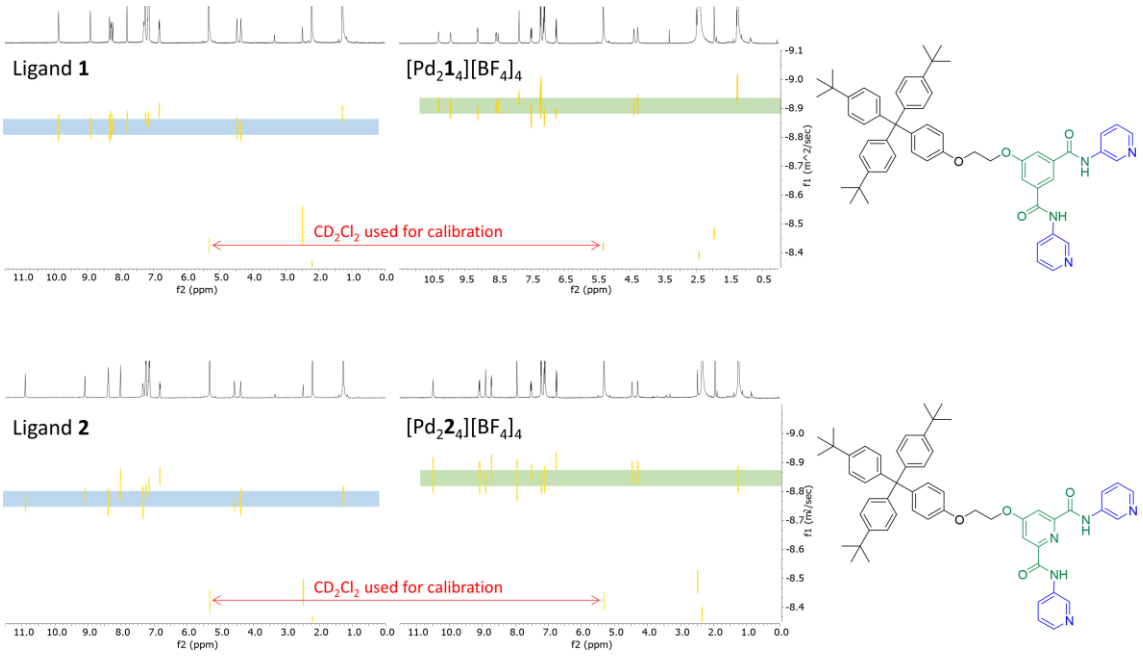

Figure S33. DOSY NMR spectra of both ligand **1** and **2** (left) and their $[Pd_2(Ligand)_4][BF_4]_4$ complexes (right). The solvent is CD_2Cl_2 with 5% dmso-d_6. Applying the Stokes-Einstein equation to the average diffusion constants of both ligands and both complexes, and assuming the weighted average viscosity of the solvents (ρ = 0.4811 g/ml, based on the molar fractions with ρ (25 °C) = 0.413 for DCM and 1.991 for DMSO) in indicate that the average radius of the complexes are 5.85 Å (Pd_2(**1**)$_4$]) and 5.97 Å (Pd_2(**2**)$_4$]) larger than those of their ligands. While this difference is on the small side, these spectra evidence that both complexes have a larger diffusion constant than their parent ligands. This is consistent with the formation of complexes that are larger than the ligand used to make the complex. Moreover, it is well-known that the measured diffusion constant can be greatly affected by some self-aggregation and by the solvation of charged species.[4] Solvation is likely different for the ligand and its complex, and some aggregation in the apolar matric of mostly CD_2Cl_2 is most likely for the ligands but not the cages (as evidenced by the dilution studies shown in Figure S38 and Figure S39).

Section S3. Titration experiments

Section S3a. Formation of Pd complexes

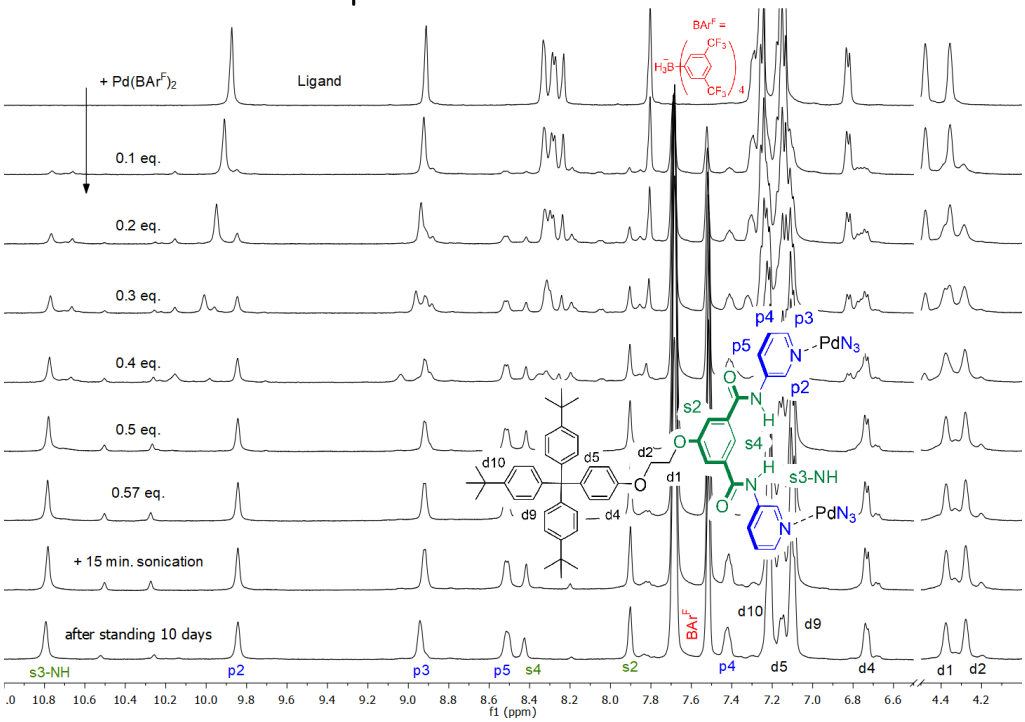

Figure S34. ^{1}H NMR spectra of a titration experiment to form [Pd$_2$**1**$_4$][BAr^F]$_4$ complex in 5% DMSO-d_6 in CD_2Cl_2 by stepwise addition of [Pd(DMSO-d_6)$_4$][BAr^F]$_2$ to **1**.

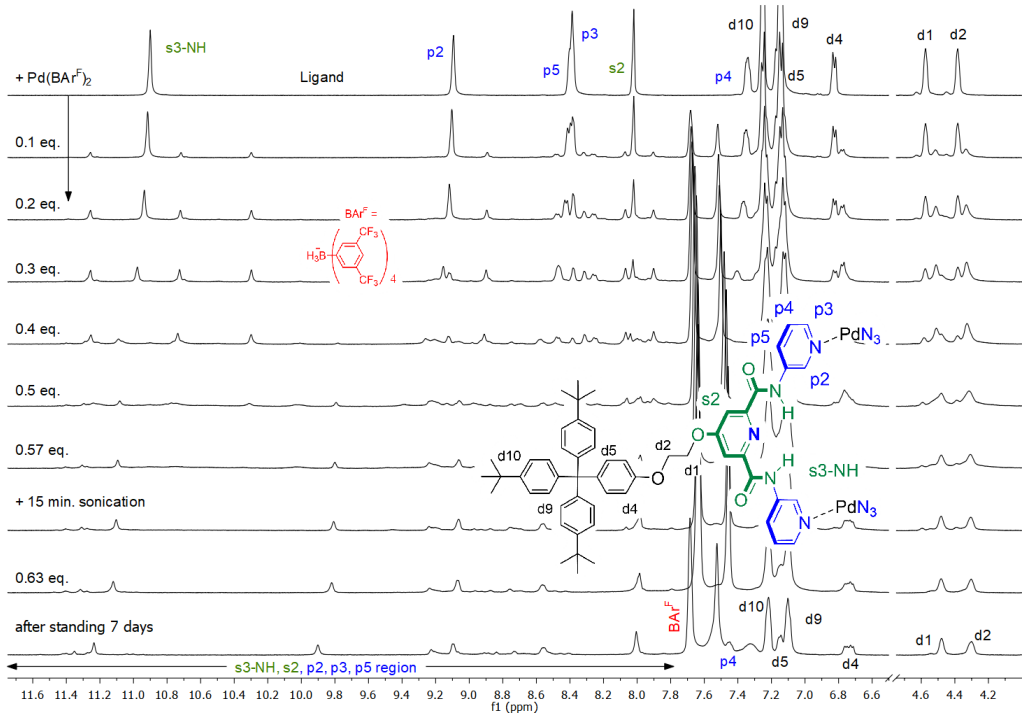

Figure S35. ^{1}H NMR spectra of a titration experiment in an attempt to form [Pd$_2$**2**$_4$][BF$_4$]$_2$ complex in 5% DMSO-d_6 in CD_2Cl_2 by stepwise addition of [Pd(DMSO-d_6)$_4$][BAr^F]$_2$ to **2**.

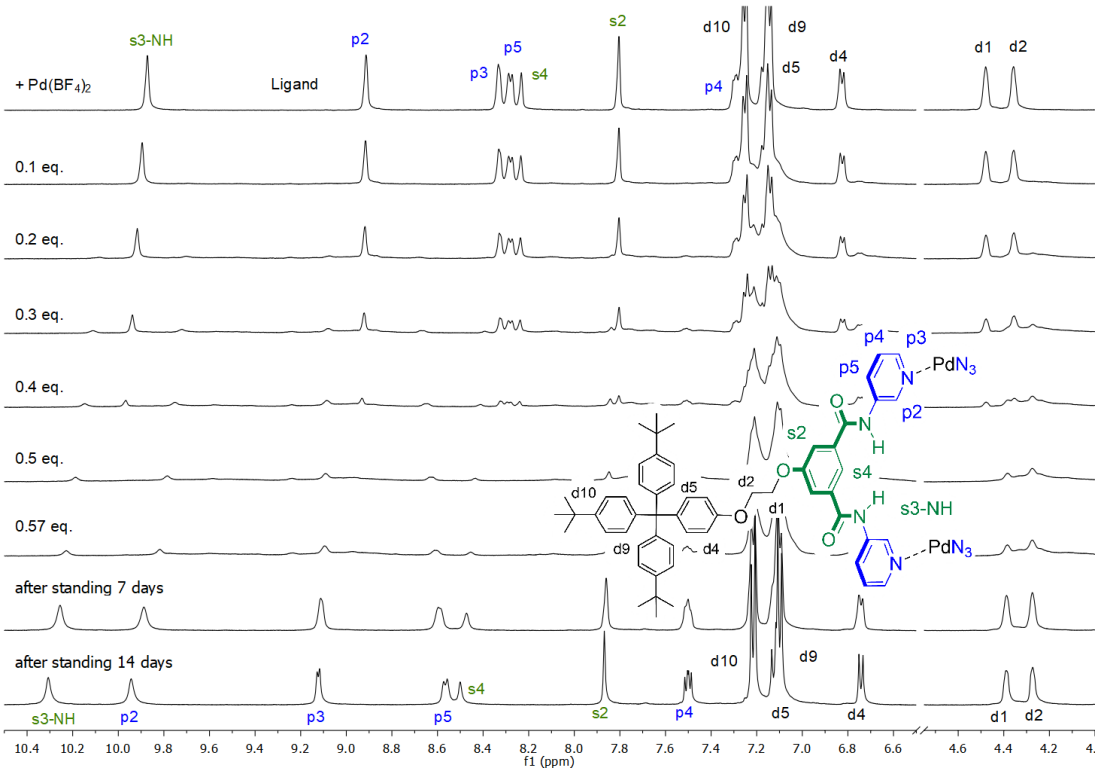

Figure S36. ^{1}H NMR spectra of a titration experiment to form $[Pd_2\mathbf{1}_4][BF_4]_4$ complex in 5% DMSO-d_6 in CD_2Cl_2 by stepwise addition of $[Pd(NCMe_3)_4][BF_4]_2$ to **1**.

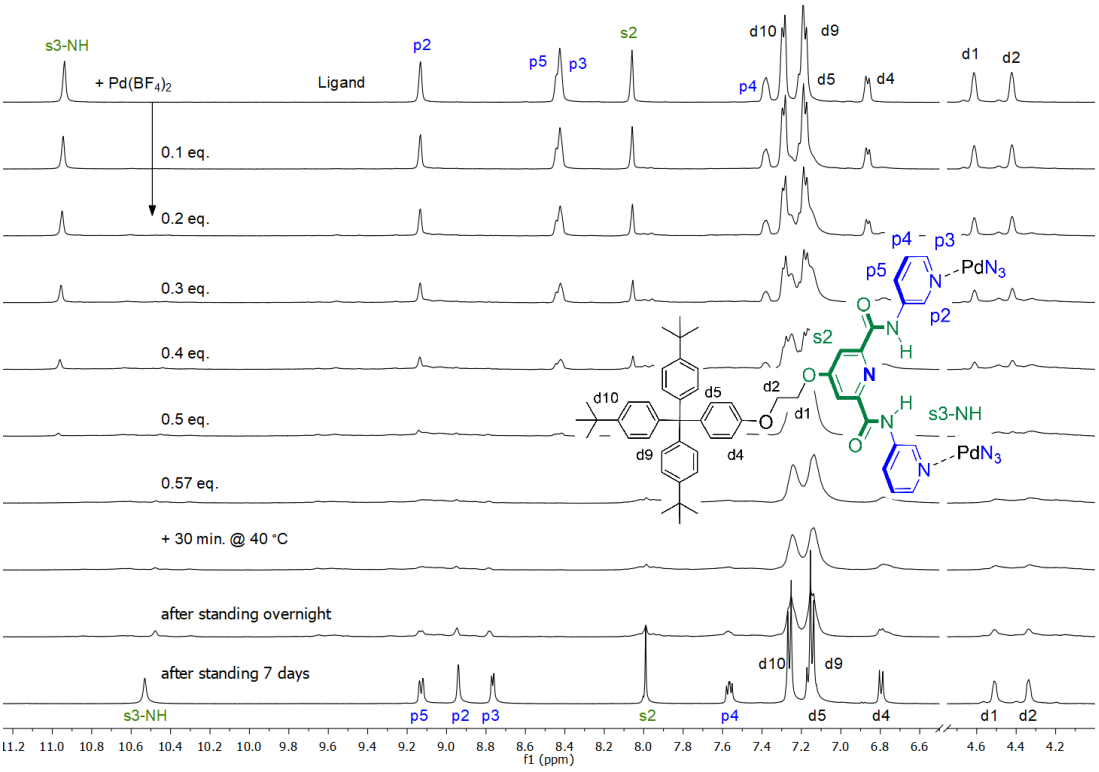

Figure S37. ^{1}H NMR spectra of a titration experiment to form $[Pd_2\mathbf{2}_4][BF_4]_4$ complex in 5% DMSO-d_6 in CD_2Cl_2 by stepwise addition of $[Pd(NCMe_3)_4][BF_4]_2$ to **2**.

Section S3b. Dilution of Pd complexes

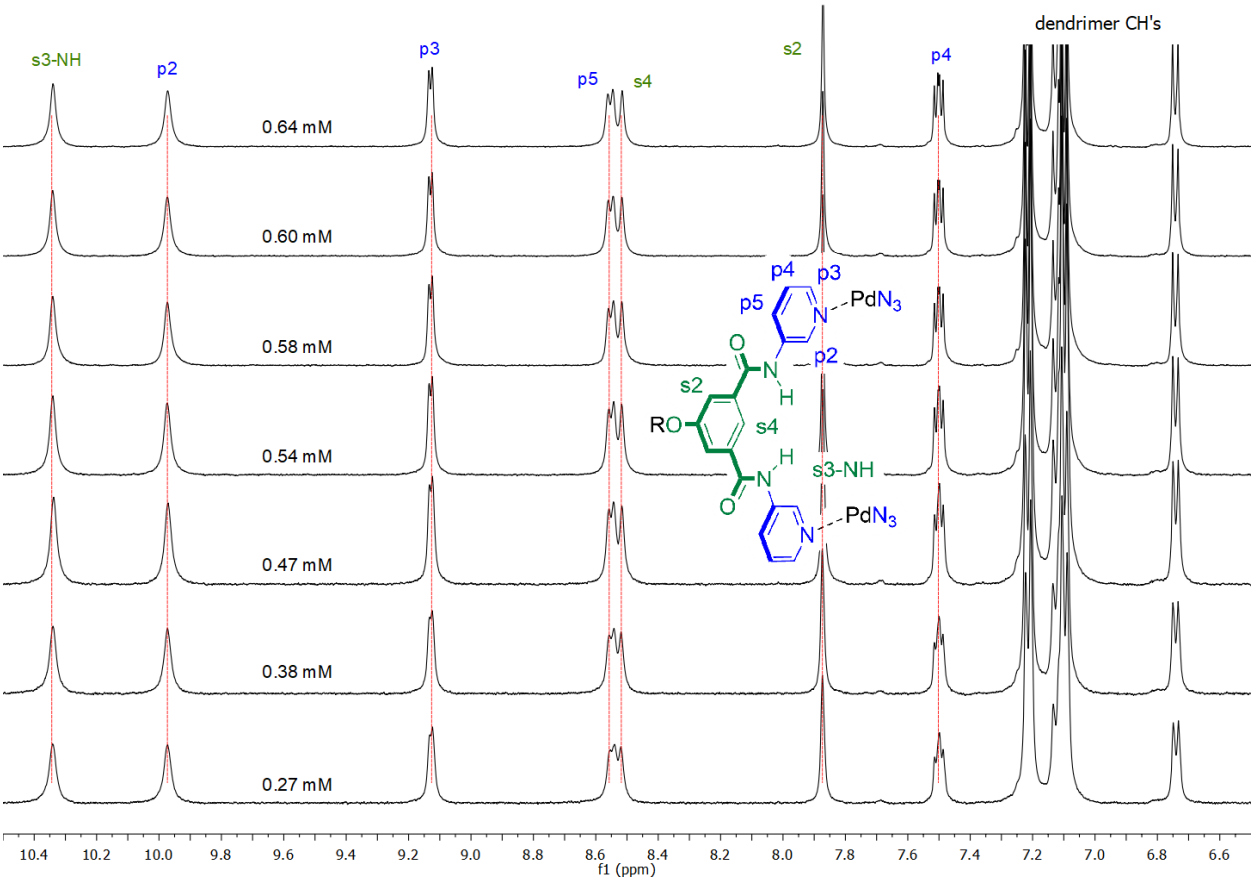

Figure S38. ^{1}H NMR spectra of a dilution study of form $[Pd_2\mathbf{1}_4][BF_4]_4$ complex in 5% DMSO-d_6 in CD_2Cl_2 in the range relevant for binding studies (0.64 – 0.27 mM) showing no significant shifting of peaks. NB: the shifts observed in a typical binding study are in the range of $|\Delta\delta| \geq 0.1$ p.p.m..

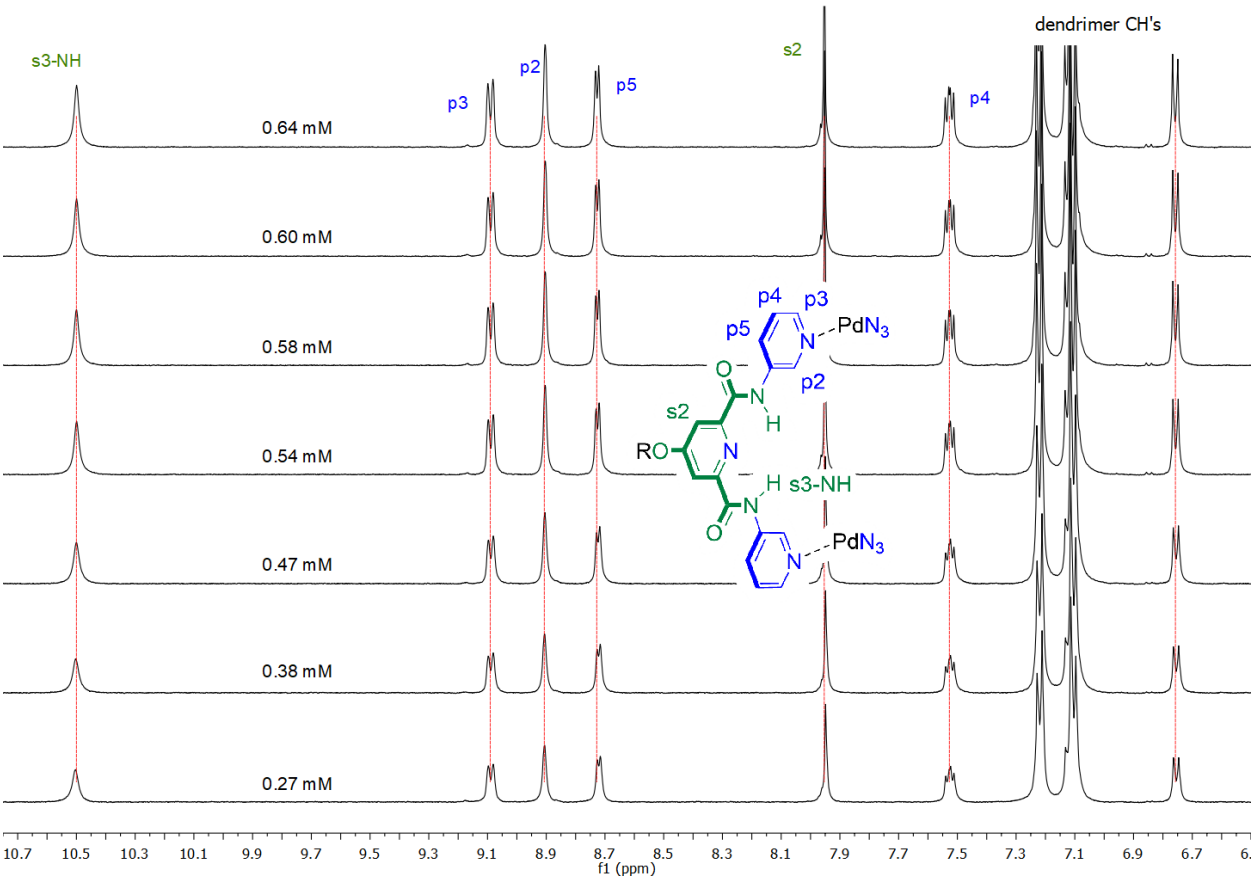

Figure S39. ^{1}H NMR spectra of a dilution study of form $[Pd_2\mathbf{2}_4][BF_4]_4$ complex in 5% DMSO-d_6 in CD_2Cl_2 in the range relevant for binding studies (0.64 – 0.27 mM) showing no significant shifting of peaks.

Section S3c. Binding studies of $[Pd_2\mathbf{1}_4][BF_4]_4$

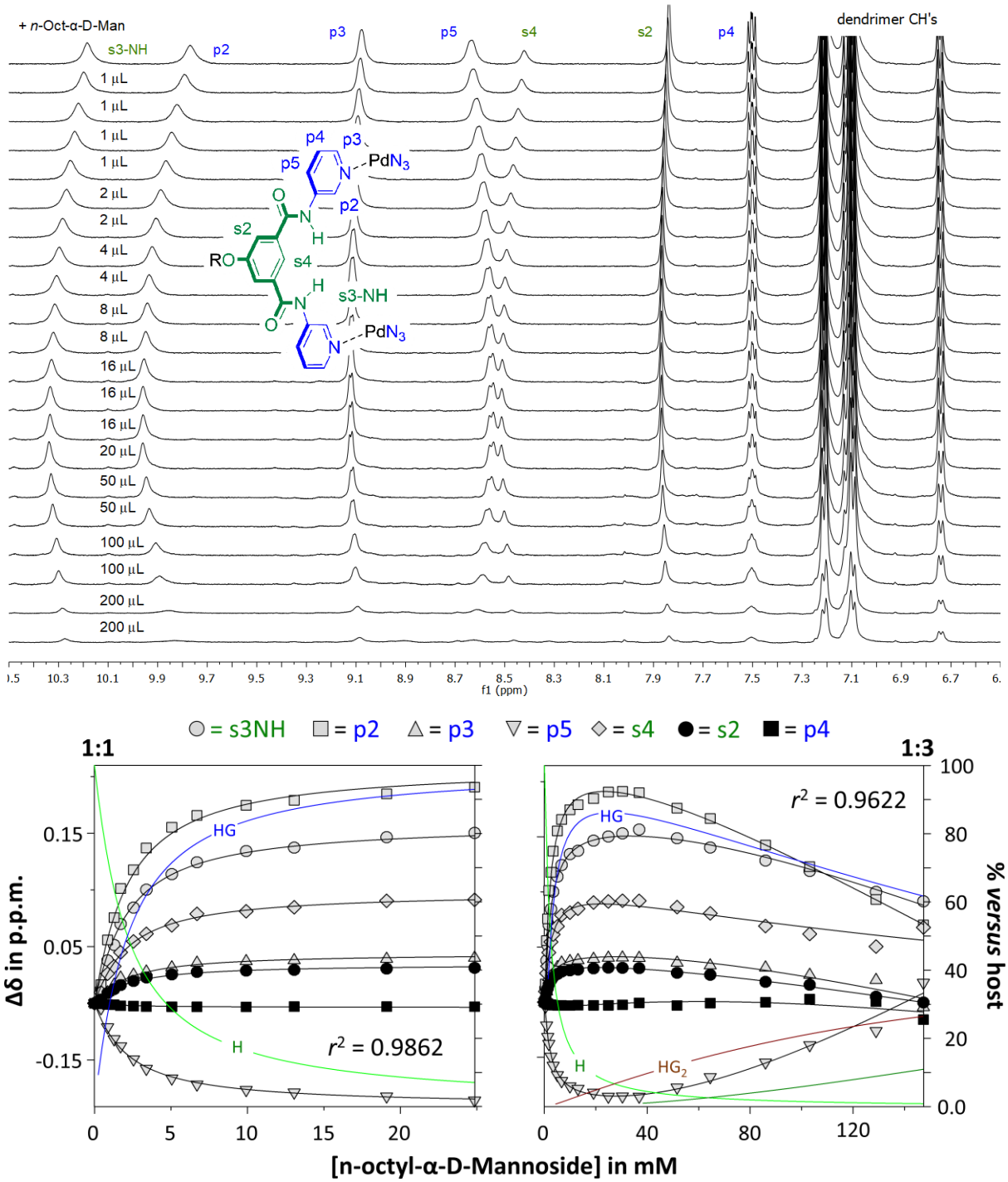

Figure S40. Top: ^{1}H NMR spectra and assignment of 0.6 mL of a 0.64 mM solution $[Pd_2\mathbf{1}_4][BF_4]_4$ to which an 258 mM solution of *n*-octyl-α-D-Mannoside **3** was added to a concentration of 147 mM. The solvent is CD_2Cl_2 with 5% DMSO-d_6. Bottom: The chemical shift differences of indicated resonances could be fitted using HypNMR. The data until 25 mM **3** could be fitted accurately (r^2 = 0.9862 over 91 data points) to a 1:1 binding model with K_a = 541 M^{-1}. Also using the data until 147 mM of **3** could be fitted with a 1:3 binding model with $K_a^{1:1}$ = 484 M^{-1} and $K_a^{1:2}$ = $K_a^{1:3}$ = 3 M^{-1} and r^2 = 0.9622 over all 147 data points. As the 1:1 binding event is nearly identical in both fits and the higher stoichiometries are negligible, we opted for using only the data until 25 mM **3** in the main text and report the main 1:1 binding with a comment that higher stoichiometries become relevant at high concentrations of **3**. Speciation is also plotted as unbound $[Pd_2\mathbf{1}_4][BF_4]_4$ (H, green) and complex bound to carbohydrate (HG, blue; HG_2, brown).

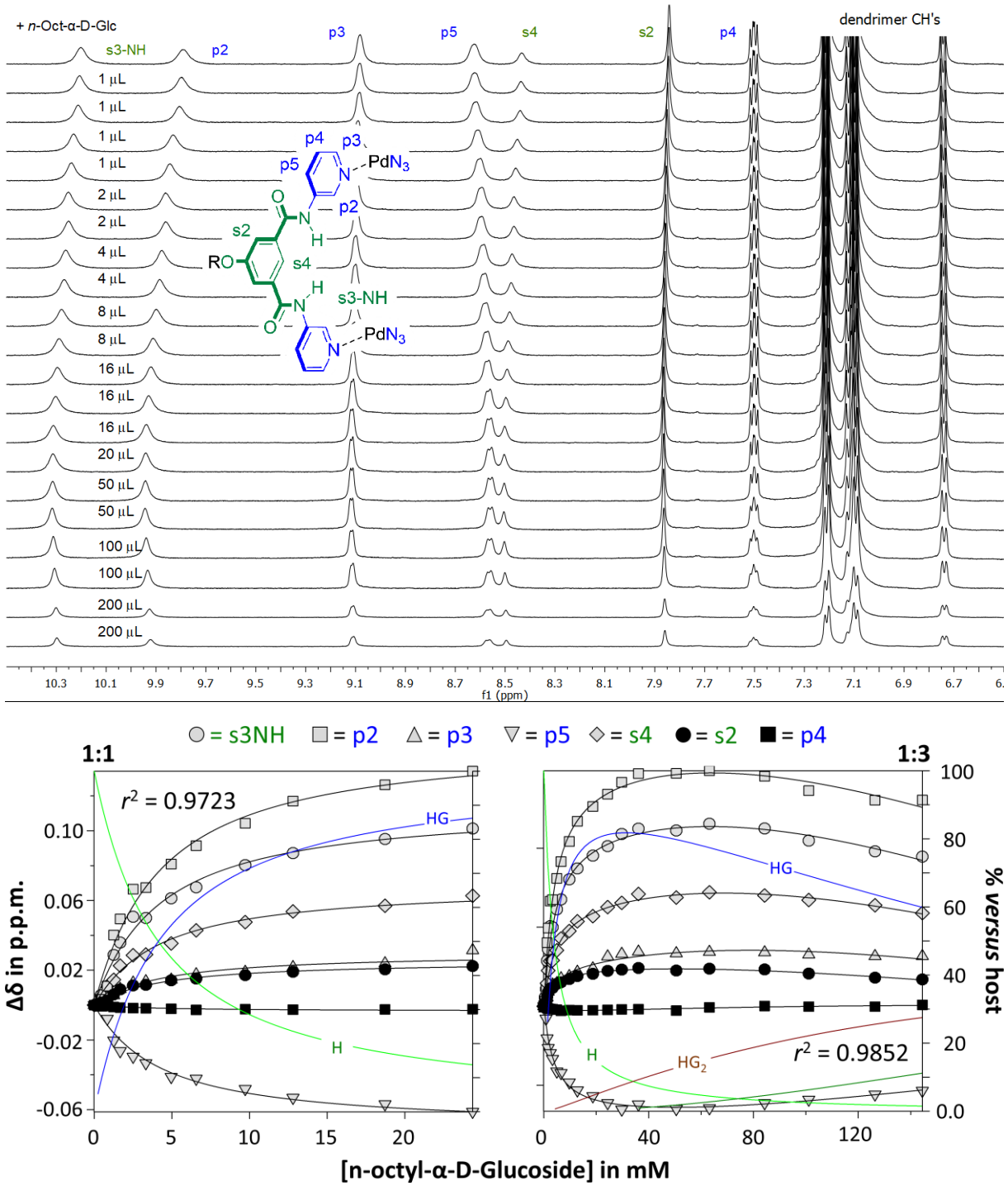

Figure S41. Top: ^{1}H NMR spectra and assignment of 0.6 mL of a 0.64 mM solution $[Pd_2\mathbf{1}_4][BF_4]_4$ to which an 253 mM solution of *n*-octyl-α-D-Glucoside **4** was added to a concentration of 144 mM. The solvent is CD_2Cl_2 with 5% DMSO-d_6. Bottom: The chemical shift differences of indicated resonances could be fitted using HypNMR. The data until 25 mM **4** could be fitted accurately (r^2 = 0.9723 over 91 data points) to a 1:1 binding model with K_a = 262 M^{-1}. Also using the data until 144 mM of **4** could be fitted with a 1:3 binding model with $K_a^{1:1}$ = 280 M^{-1} and $K_a^{1:2}$ = $K_a^{1:3}$ = 3 M^{-1} and r^2 = 0.9852 over all 147 data points. As the 1:1 binding event is nearly identical in both fits and the higher stoichiometries are negligible, we opted for using only the data until 25 mM **4** in the main text and report the main 1:1 binding with a comment that higher stoichiometries become relevant at high concentrations of **4**. Speciation is also plotted as unbound $[Pd_2\mathbf{1}_4][BF_4]_4$ (H, green) and complex bound to carbohydrate (HG, blue; HG_2, brown).

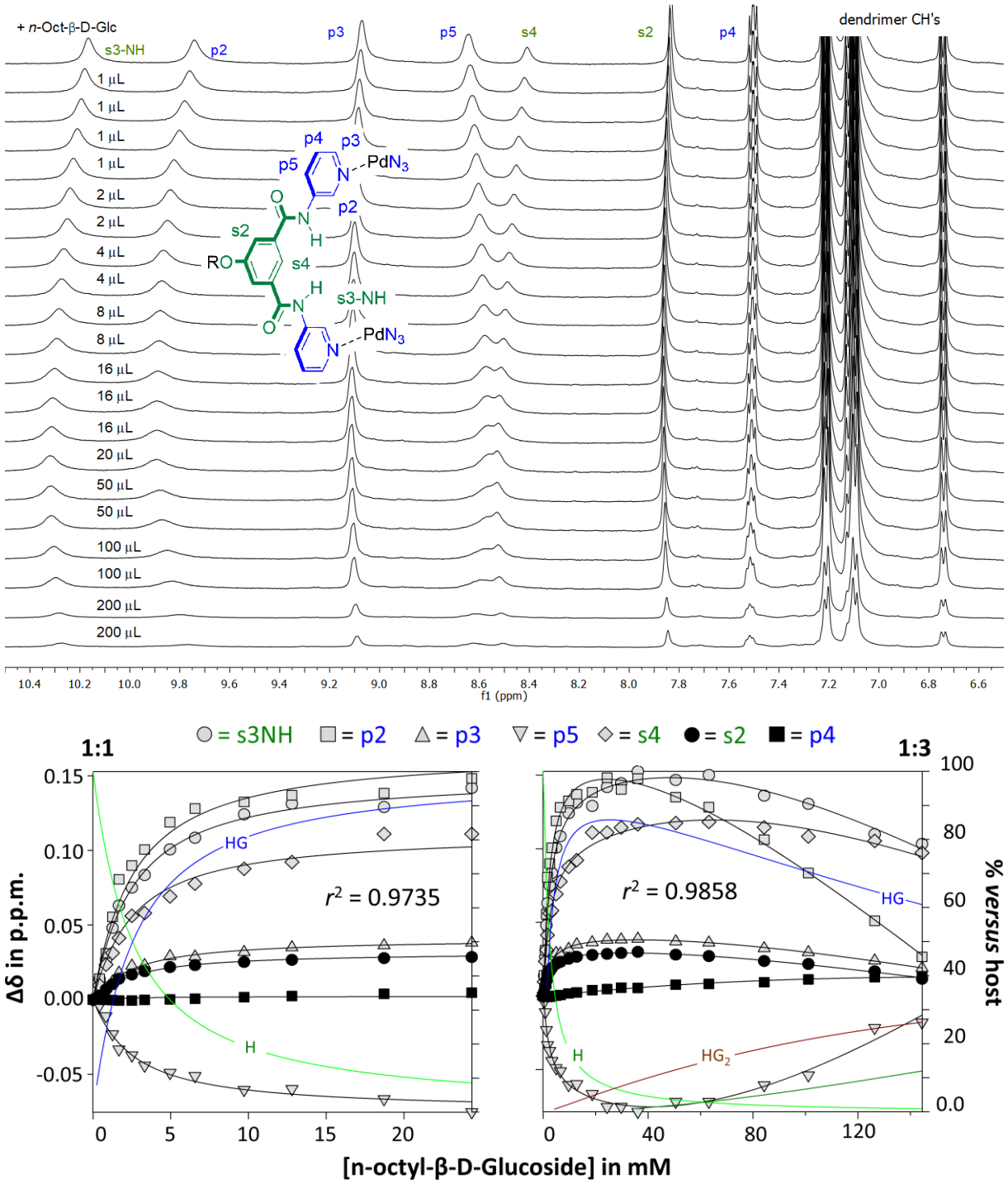

Figure S42. Top: ^{1}H NMR spectra and assignment of 0.6 mL of a 0.64 mM solution $[Pd_2\mathbf{1}_4][BF_4]_4$ to which an 253 mM solution of *n*-octyl-β-D-Glucoside **5** was added to a concentration of 144 mM. The solvent is CD_2Cl_2 with 5% DMSO-d_6. Bottom: The chemical shift differences of indicated resonances could be fitted using HypNMR. The data until 25 mM **5** could be fitted accurately (r^2 = 0.9735 over 91 data points) to a 1:1 binding model with K_a = 447 M^{-1}. Also using the data until 144 mM of **5** could be fitted with a 1:3 binding model with $K_a^{1:1}$ = 471 M^{-1} and $K_a^{1:2}$ = $K_a^{1:3}$ = 3 M^{-1} and r^2 = 0.9858 over all 147 data points. As the 1:1 binding event is nearly identical in both fits and the higher stoichiometries are negligible, we opted for using only the data until 25 mM **5** in the main text and report the main 1:1 binding with a comment that higher stoichiometries become relevant at high concentrations of **5**. Speciation is also plotted as unbound $[Pd_2\mathbf{1}_4][BF_4]_4$ (H, green) and complex bound to carbohydrate (HG, blue; HG_2, brown).

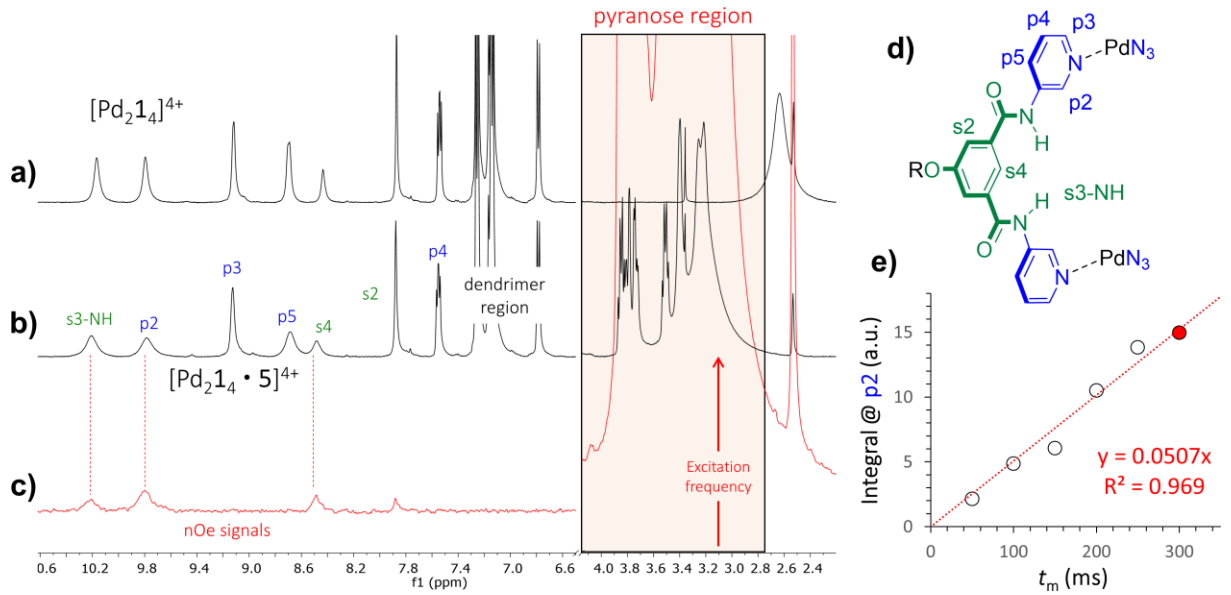

Figure S43. a) 2.5 mM solution of $[Pd_2\mathbf{1}_4][BF_4]_4$ in CD_2Cl_2 with 5% dmso-d_6; b) idem as 'a', but also containing 15 mM *n*-octyl-β-D-glucoside **5**; c) 1D-selective nOe spectrum recorded of the solution in 'b' after excitation at 3.1 p.p.m. in the pyranose region (t_m = 300 ms), showing nOe signals with the inwards facing **s3-NH**, **p2** and **s4**; d) schematic representation and labeling of $[Pd_2\mathbf{1}_4]4+$; e) plot of the integral (in arbitrary units) of the nOe signal of **p2** as a function of the mixing time (t_m). The linear relationship evidences that spin diffusion is insignificant at the mixing time used (300 ms).

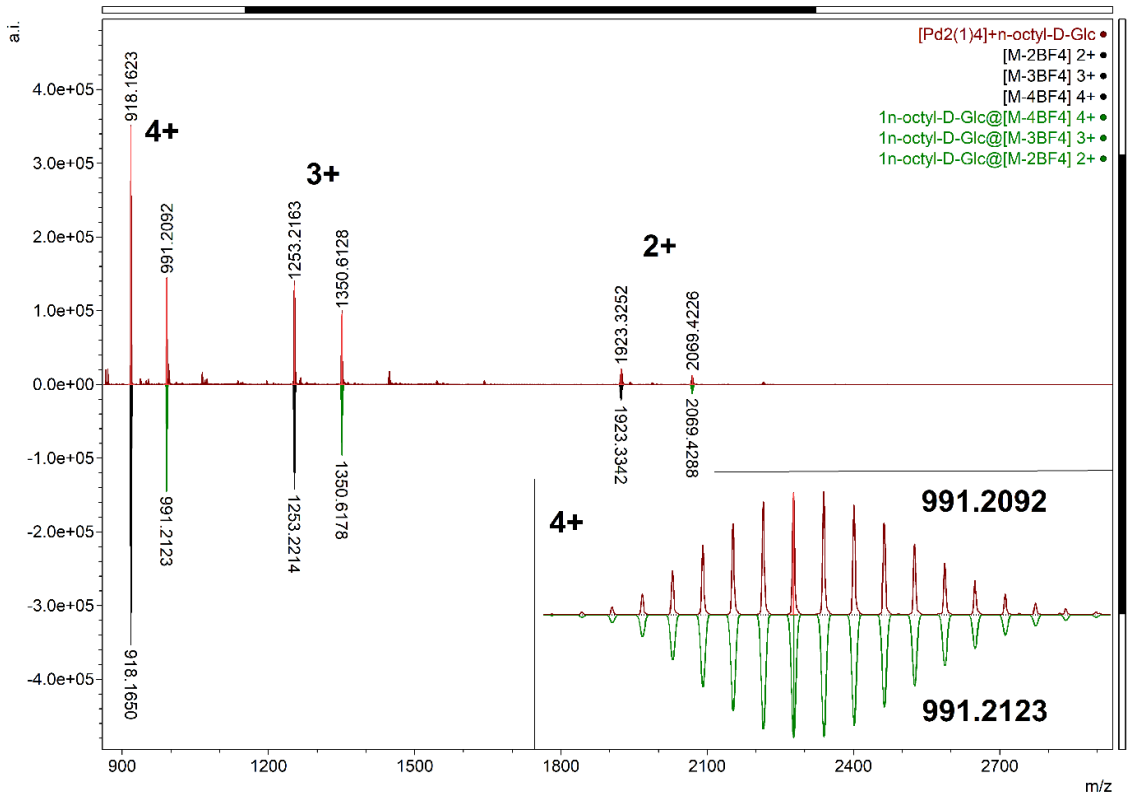

Figure S44. ESI-MS spectrum of $[Pd_2\mathbf{1}_4]^{4+}$ and its BF_4^- adducts in the presence of *n*-octyl-β-D-glucoside **5** as measured (top) and simulated (bottom). The inset figure shows the measured and simulated monoisotopic mass distribution of the largest peak containing **5**, $[Pd_2\mathbf{1}_4 \cdot \mathbf{5}]^{4+}$.

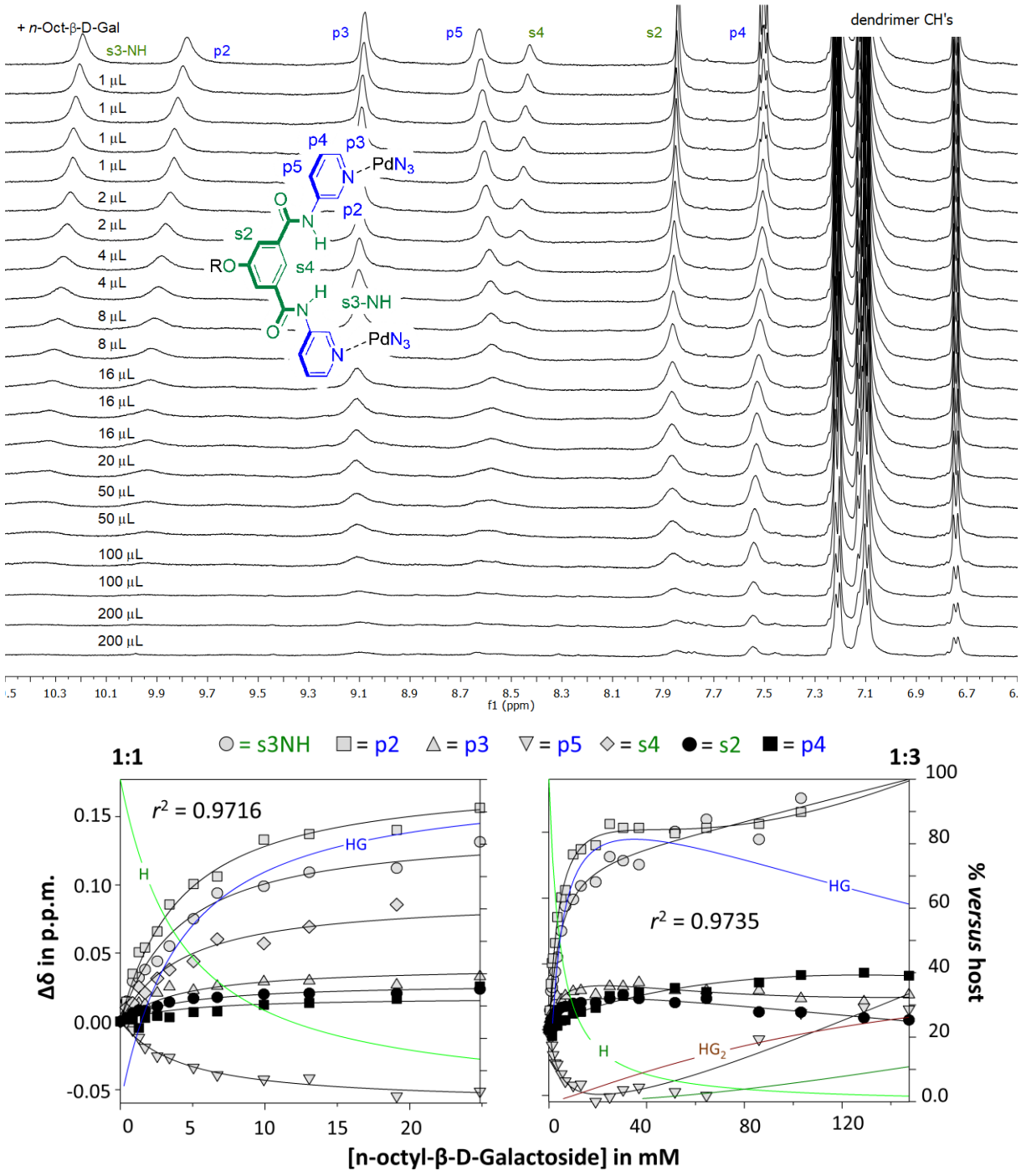

Figure S45. Top: ^{1}H NMR spectra and assignment of 0.6 mL of a 0.64 mM solution $[Pd_2\mathbf{1}_4][BF_4]_4$ to which an 256 mM solution of *n*-octyl-β-D-Galactoside **6** was added to a concentration of 147 mM. The solvent is CD_2Cl_2 with 5% DMSO-d_6. Bottom: The chemical shift differences of indicated resonances could be fitted using HypNMR. The data until 25 mM **6** could be fitted accurately (r^2 = 0.9716 over 90 data points) to a 1:1 binding model with K_a = 262 M^{-1}. Also using the data until 144 mM of **6** could be fitted with a 1:3 binding model with $K_a^{1:1}$ = 244 M^{-1} and $K_a^{1:2}$ = $K_a^{1:3}$ = 3 M^{-1} and r^2 = 0.9735 over all 134 data points. As the 1:1 binding event is nearly identical in both fits and the higher stoichiometries are negligible, we opted for using only the data until 25 mM **6** in the main text and report the main 1:1 binding with a comment that higher stoichiometries become relevant at high concentrations of **6**. Speciation is also plotted as unbound $[Pd_2\mathbf{1}_4][BF_4]_4$ (H, green) and complex bound to carbohydrate (HG, blue; HG_2, brown). NB: the resonances broadened significantly, but were sharpened when nitrate was added, as detailed in Figure S46.

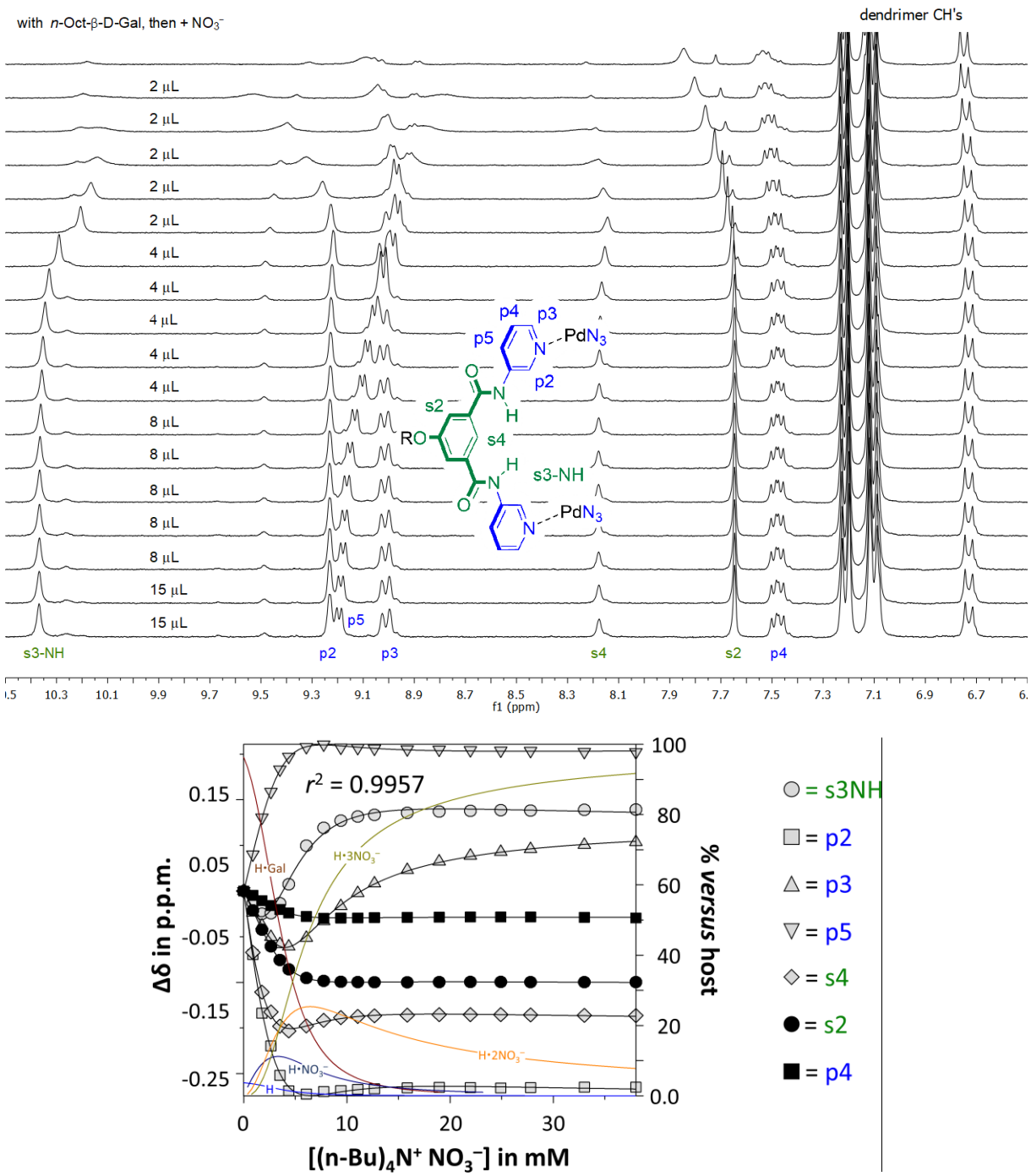

Figure S46. Top: ^{1}H NMR spectra of a solution of 0.6 mL 0.74mM $[Pd_2\mathbf{1}_4][BF_4]_4$ with 99 mM *n*-octyl-β-D-Galactoside **6** (about the same as final point in the titration, see Figure S45), that was titrated with a 266 mM solution of $(n\text{-}Bu)_4N^+NO_3^-$. The solvent is CD_2Cl_2 with 5% DMSO-d_6. Bottom: The chemical shift differences of indicated resonances could be modelled using HypNMR. The model incorporated the presence of **6** and the 1:1 binding constant of $[Pd_2\mathbf{1}_4]^{4+}$ for **6** determined here (Figure S45, K_a = 262 M^{-1}) and also incorporated a 2:1 complex:NO_3^- stoichiometry of 100 M^{-1} that has been required in a similar system.[5] The data was thus further modelled with a 1:3 complex: NO_3^- stoichiometry with $K_a^{1:1}$ = 1,862 M^{-1}, $K_a^{1:2}$ = 5370 and $K_a^{1:3}$ = 3160 M^{-1} and r^2 = 0.9957 over all 126 data points. Speciation is also plotted as unbound $[Pd_2\mathbf{1}_4][BF_4]_4$ (H, blue), the complex bound to **6** (H•Gal, brown), and the complex bound to one nitrate (dark blue), two nitrate (orange) and three nitrate (gold).

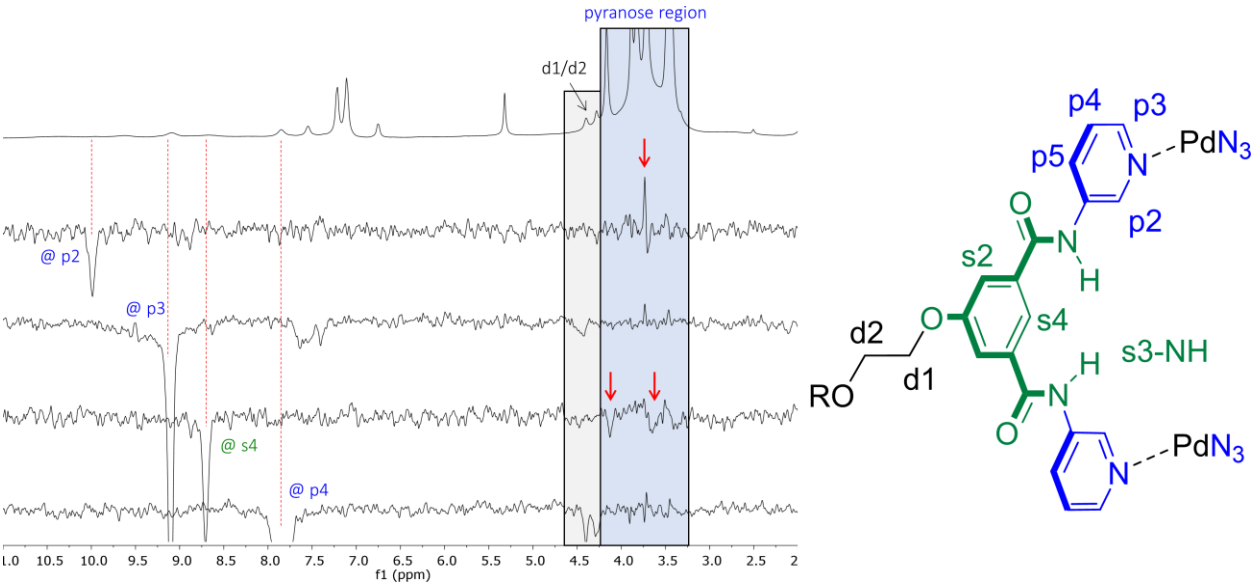

Figure S47. 1D-selective nOe studies (t_m = 350 ms) of a 2.3 mM solution of $[Pd_2\mathbf{1}_4][BF_4]_4$ containing 100 mM *n*-octyl-β-D-Galactoside **6**. Irradiation of a frequency representative of the inwards facing **p2** and **s4** gave the clearest nOe signals in the pyranose region (indicated with red arrows) as opposed to irradiation of the outwards facing **p3** and **p4**. See also Figure S45 for the titration, the concentration of **6** is similar in the spectrum after the first 100 µL addition.

Section S3d. Binding studies of $[Pd_2\mathbf{2}_4][BF_4]_4$

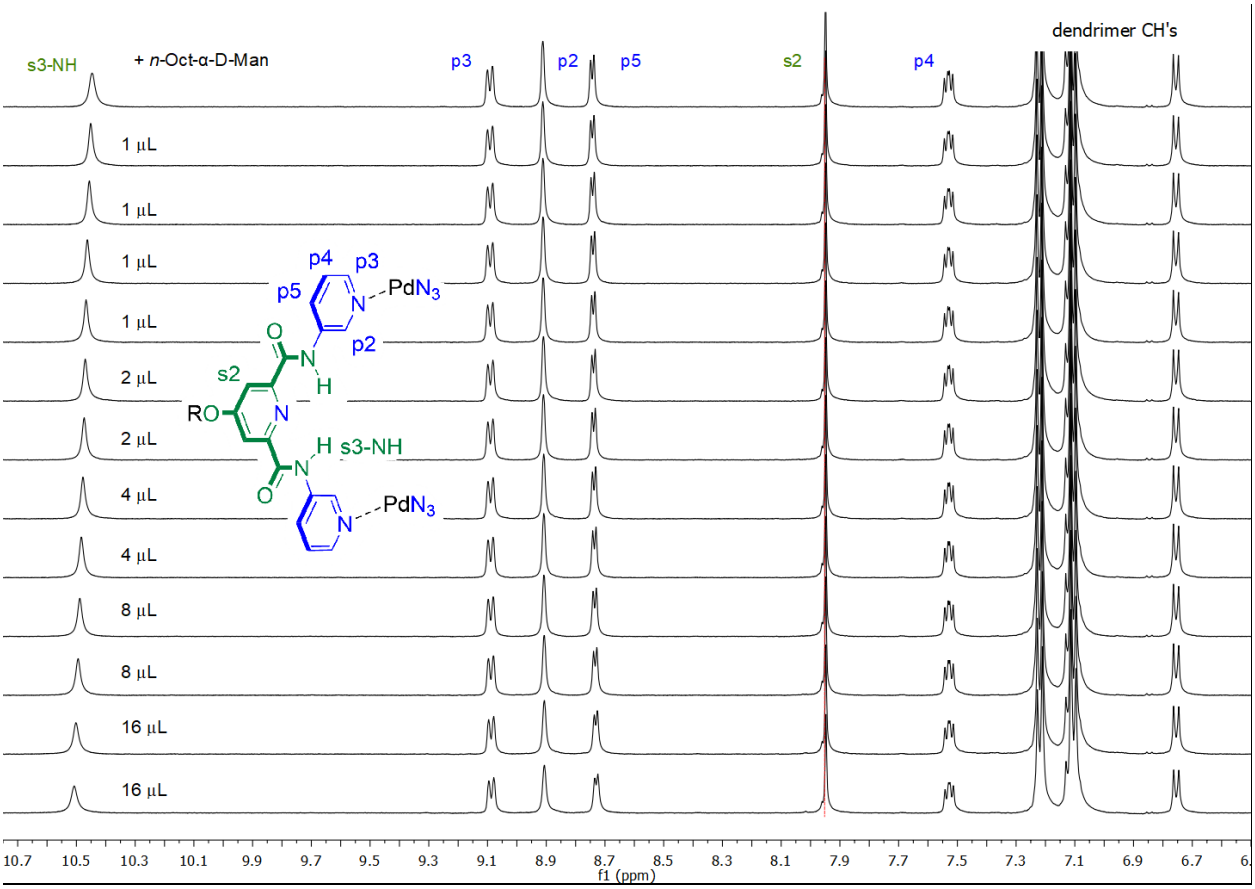

Figure S48. ^{1}H NMR spectra and assignment of 0.6 mL of a 0.64 mM solution $[Pd_2\mathbf{2}_4][BF_4]_4$ to which an 258 mM solution of *n*-octyl-α-D-Mannoside **3** was added (solvent = CD_2Cl_2 with 5% DMSO-d_6) The spectra shown are to a total concentration of 25 mM **3** revealing only marginal peak shifting (**p2** was particularly stationary). This contrasts sharply with the titration of $[Pd_2\mathbf{1}_4][BF_4]_4$ with **3**, where saturation is evident at 25 mM of **3** (see Figure S40). As a result, these spectra were interpreted as evidence for non-binding (or at least binding that is much weaker than observed with $[Pd_2\mathbf{1}_4][BF_4]_4$).

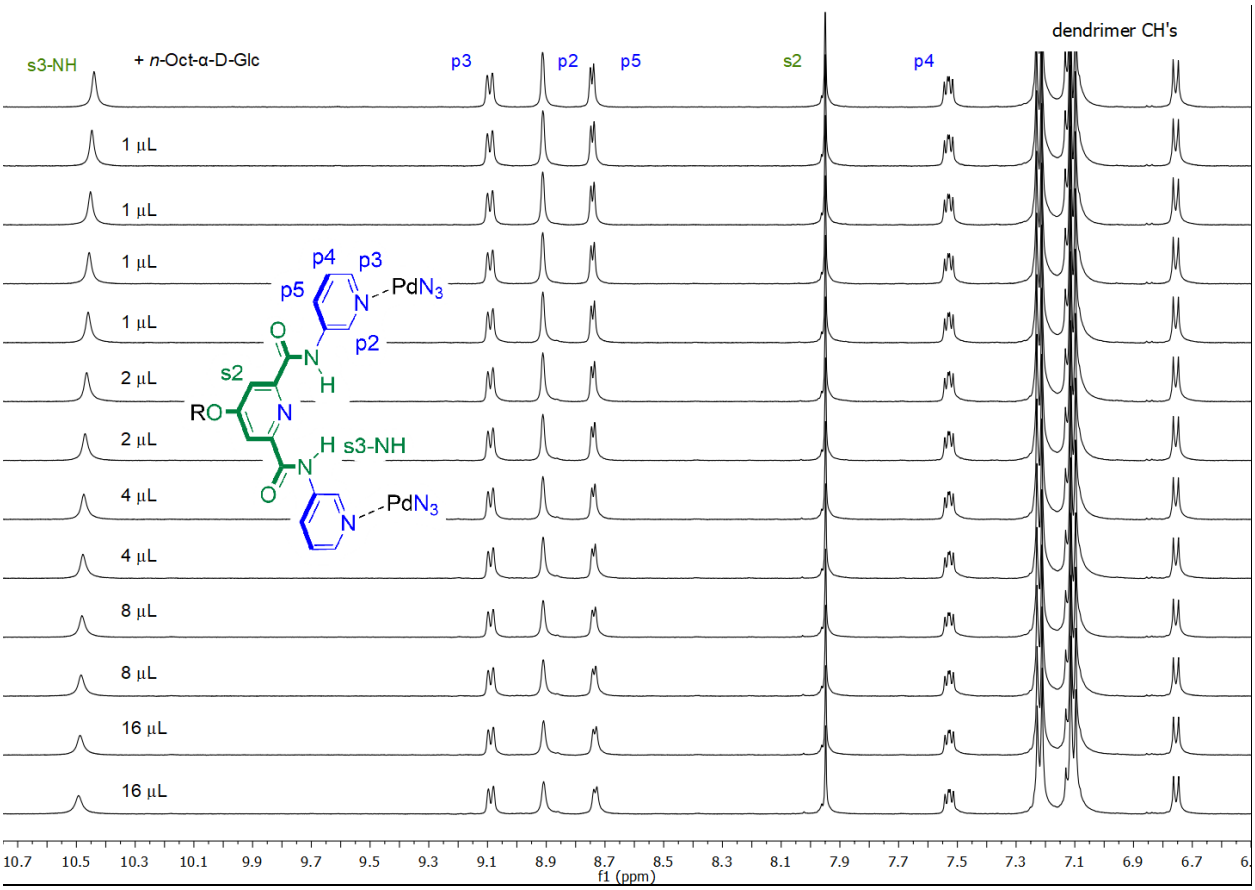

Figure S49. ^{1}H NMR spectra and assignment of 0.6 mL of a 0.64 mM solution $[Pd_2\mathbf{2}_4][BF_4]_4$ to which an 253 mM solution of *n*-octyl-α-D-Glucoside **4** was added (solvent = CD_2Cl_2 with 5% DMSO-d_6) The spectra shown are to a total concentration of 25 mM **4** revealing only marginal peak shifting (**p2** was particularly stationary). This contrasts sharply with the titration of $[Pd_2\mathbf{1}_4][BF_4]_4$ with **4**, where saturation is evident at 25 mM of **4** (see Figure S41). As a result, these spectra were interpreted as evidence for non-binding (or at least binding that is much weaker than observed with $[Pd_2\mathbf{1}_4][BF_4]_4$).

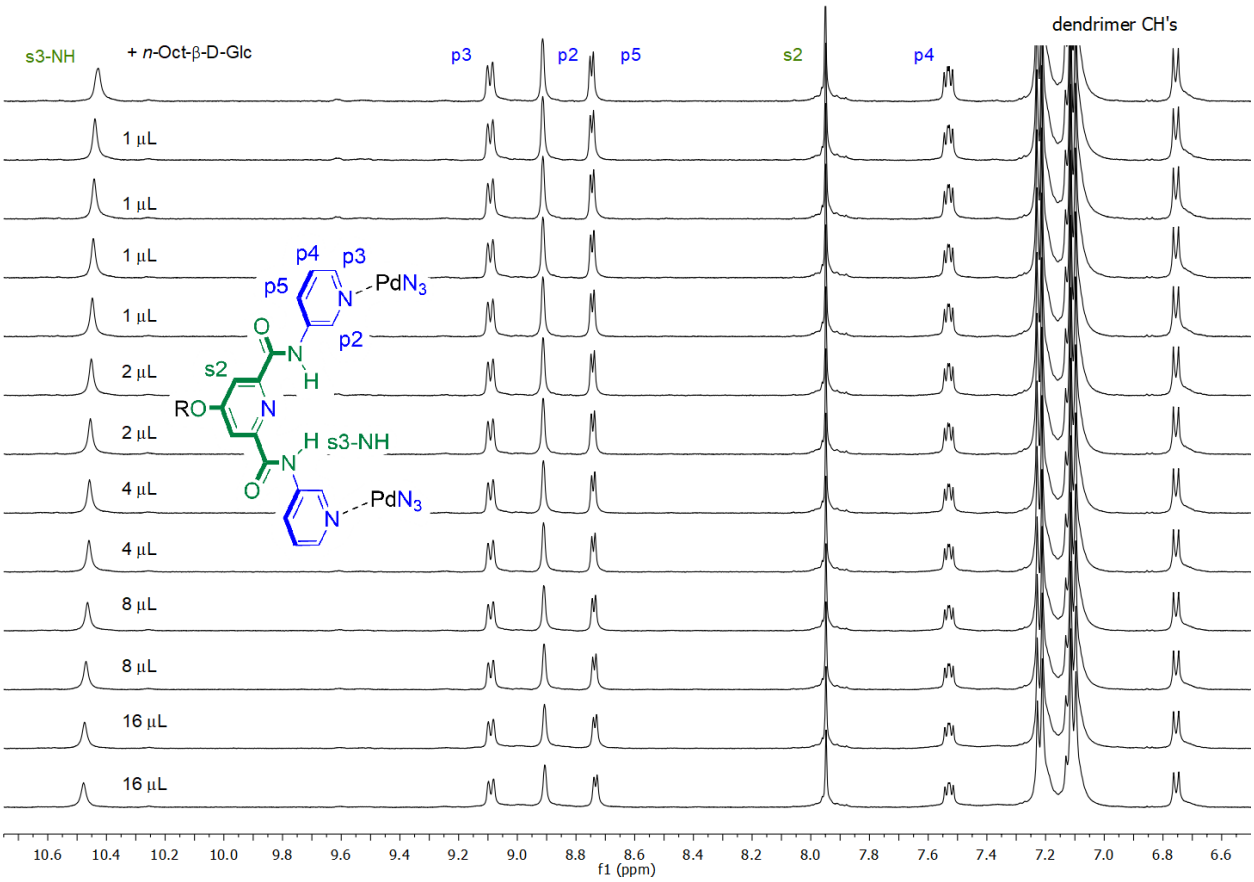

Figure S50. ^{1}H NMR spectra and assignment of 0.6 mL of a 0.64 mM solution $[Pd_2\mathbf{2}_4][BF_4]_4$ to which an 253 mM solution of *n*-octyl-β-D-Glucoside **5** was added (solvent = CD_2Cl_2 with 5% DMSO-d_6) The spectra shown are to a total concentration of 25 mM **5** revealing only marginal peak shifting (**p2** was particularly stationary). This contrasts sharply with the titration of $[Pd_2\mathbf{1}_4][BF_4]_4$ with **5**, where saturation is evident at 25 mM of **5** (see Figure S42). As a result, these spectra were interpreted as evidence for non-binding (or at least binding that is much weaker than observed with $[Pd_2\mathbf{1}_4][BF_4]_4$).

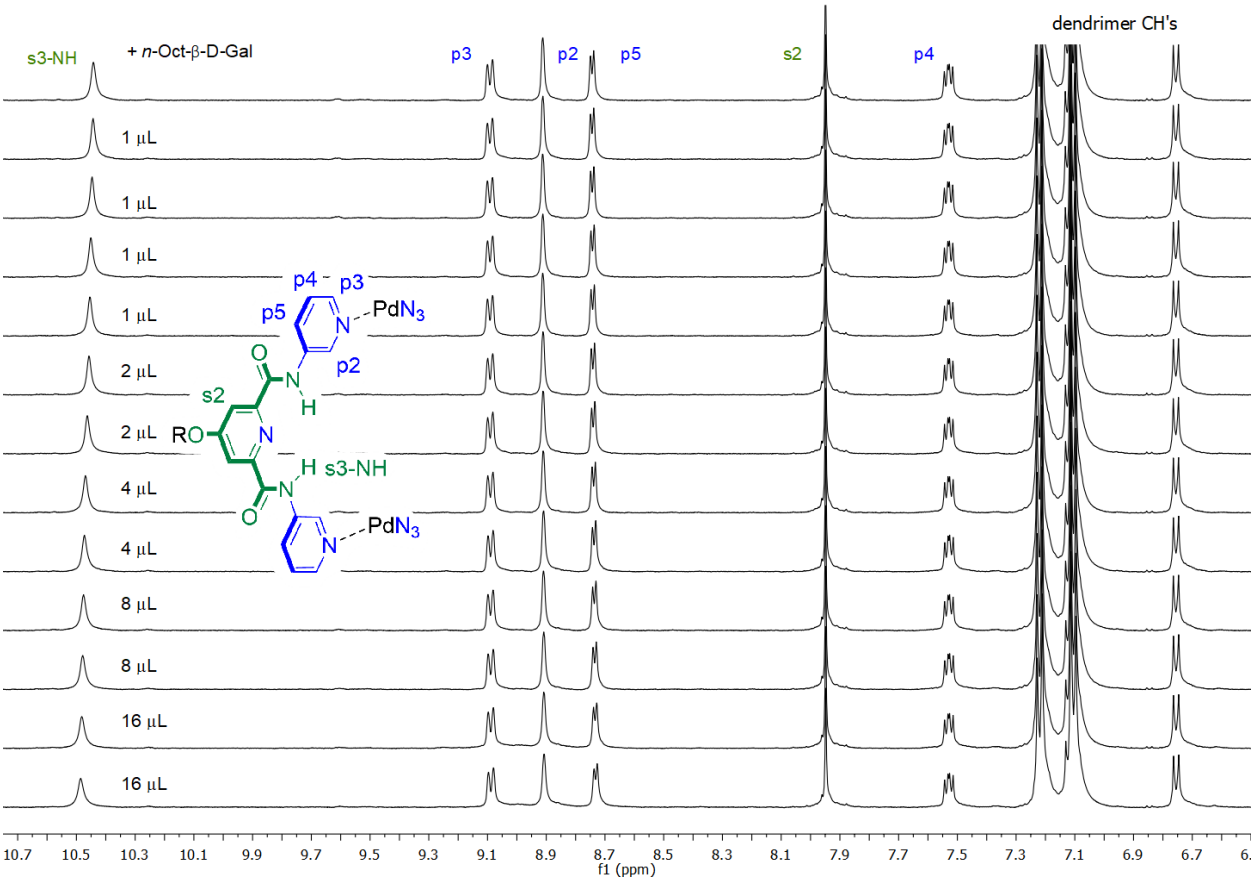

Figure S51. ^{1}H NMR spectra and assignment of 0.6 mL of a 0.64 mM solution $[Pd_2\mathbf{2}_4][BF_4]_4$ to which an 258 mM solution of *n*-octyl-β-D-Galactoside **6** was added (solvent = CD_2Cl_2 with 5% DMSO-d_6) The spectra shown are to a total concentration of 25 mM **6** revealing only marginal peak shifting (**p2** was particularly stationary). This contrasts sharply with the titration of $[Pd_2\mathbf{1}_4][BF_4]_4$ with **6**, where saturation is evident at 25 mM of **6** (see Figure S45). As a result, these spectra were interpreted as evidence for non-binding (or at least binding that is much weaker than observed with $[Pd_2\mathbf{1}_4][BF_4]_4$).

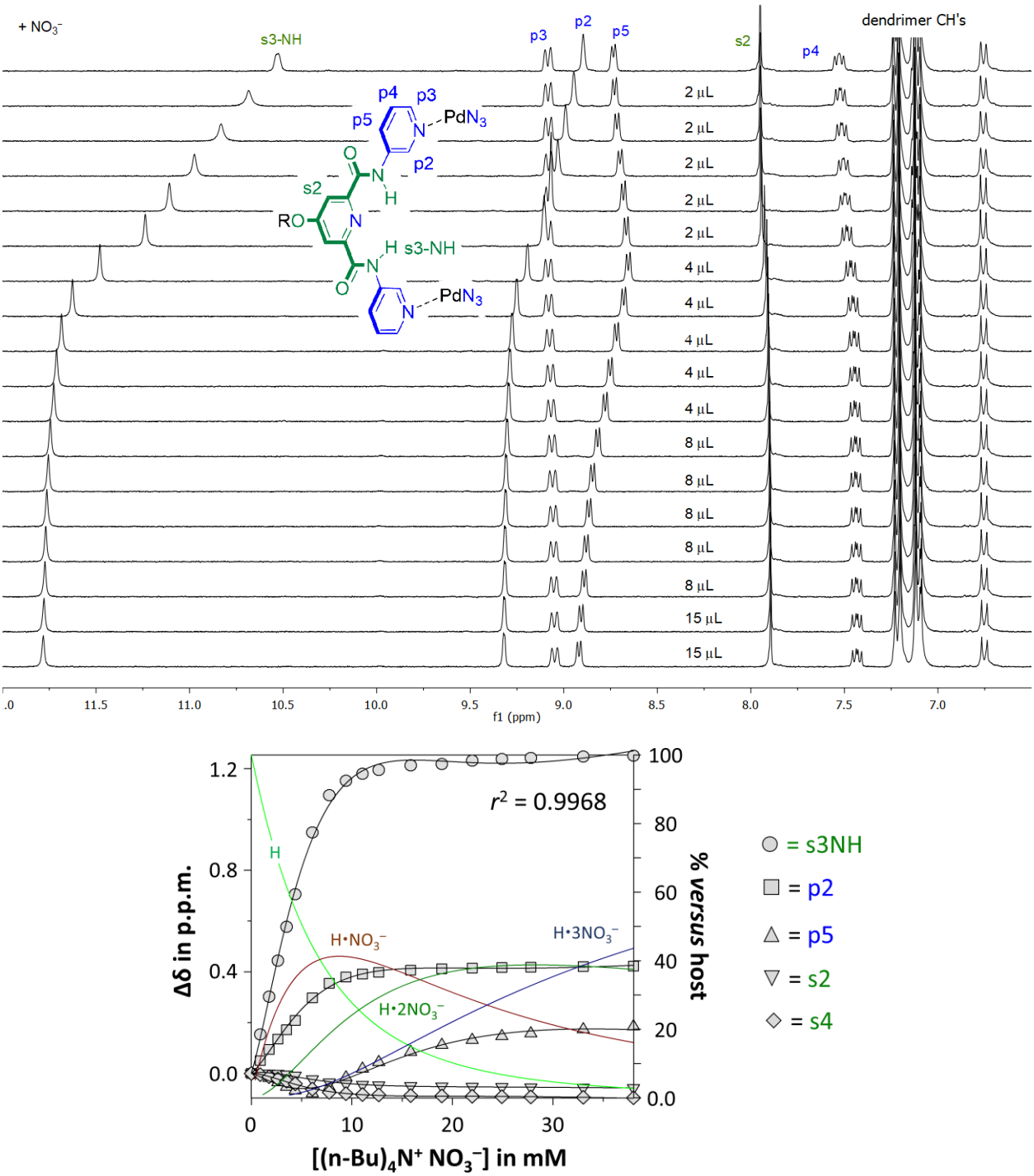

Figure S52. Top: ^{1}H NMR spectra and assignment of 0.6 mL of a 0.64 mM solution $[Pd_2\mathbf{2}_4][BF_4]_4$ to which an 266 mM solution of $(n\text{-}Bu)_4N^+NO_3^-$ was added. The solvent is CD_2Cl_2 with 5% DMSO-d_6. Bottom: The chemical shift differences of indicated resonances could be modelled using HypNMR. The model incorporated a 2:1 complex:NO_3^- stoichiometry of 100 M^{-1} that has been required in a similar system.[5] The data was thus further modelled with a 1:3 complex: NO_3^- stoichiometry with $K_a^{1:1}$ = 159 M^{-1}, $K_a^{1:2}$ = 63 and $K_a^{1:3}$ = 31 M^{-1} and r^2 = 0.9978 over all 90 data points. Speciation is also plotted as unbound $[Pd_2\mathbf{1}_4][BF_4]_4$ (H, light green) and the complex bound to one nitrate (brown), two nitrate (dark green) and three nitrate (dark blue). **NB:** nitrate binding with $[Pd_2\mathbf{2}_4][BF_4]_4$ is thus two orders of magnitude weaker than nitrate binding to $[Pd_2\mathbf{1}_4][BF_4]_4$ (with $K_a^{1:1}$ = 13,490 M^{-1} see Figure S46). This is also consistent with the lack of binding observed between $[Pd_2\mathbf{2}_4][BF_4]_4$ and carbohydrates.

Section S4. Computational details

Computations were done using Spartan 2018 running on 32 cores operating at 4 GHz and done at the ωB97X-D / 6-31G* level of theory (*in vacuo*) for calculations using density functional theory (DFT). Initial geometries were drawn in Spartan and allowed to geometry optimize without any constraints. Models were rendered using PyMol.

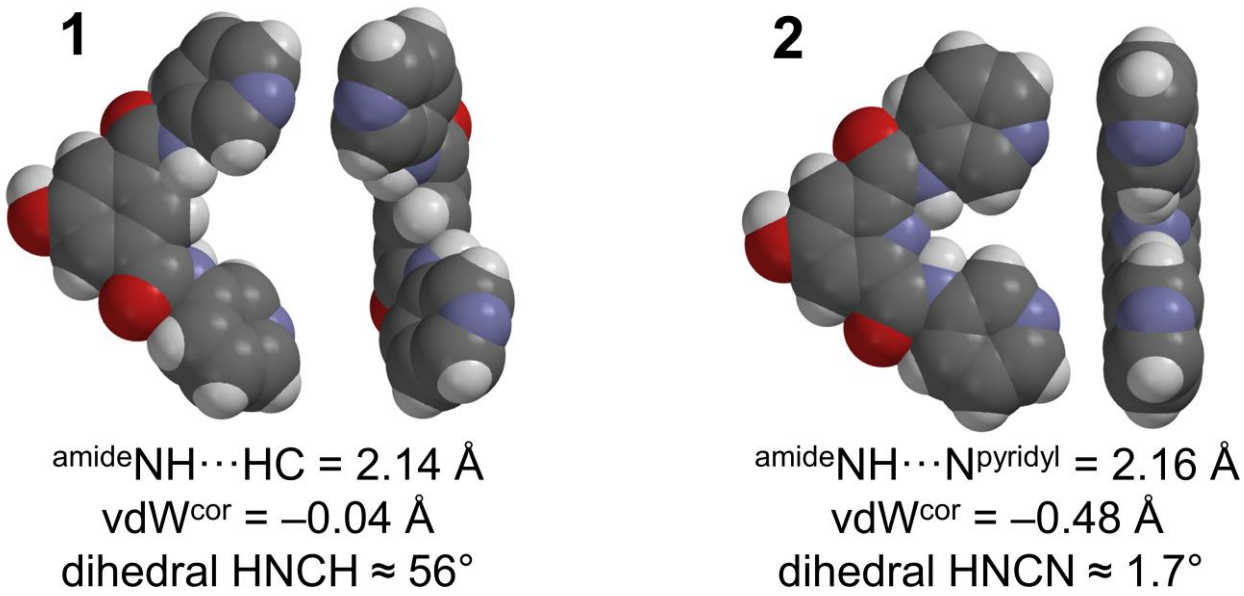

Figure S53. Geometry optimized molecular models of ligands **1** and **2** to visualize the steric clash in **1** and the preorganizing feature of **2**. The van der Waals corrected distances (vdW^{corr}) are the indicated intramolecular distances minus the van der Waals radii of the atoms in close contact (H = 1.09 Å and N = 1.55 Å).

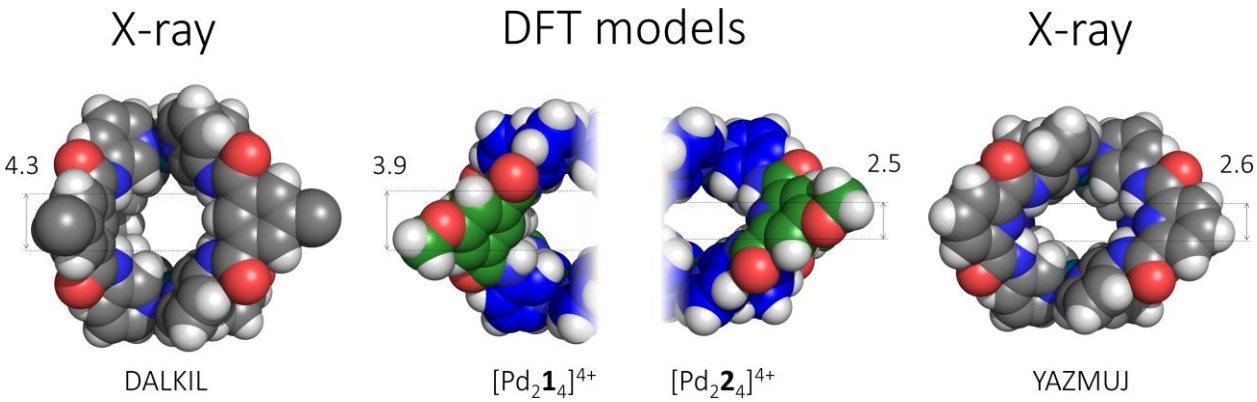

Figure S54. Comparison of the two DFT-generated models (centre) to very similar complexes extracted from crystal structures with indicated refcodes. The interior heights of the structures is calculated by measuring by the distance between the H4 centroids consisting of the inwards facing CH H's of the Pd(pyridyl)$_4$ moieties and subtracting twice the van der Waals radius of hydrogen (1.09 Å). Distances are in Å.

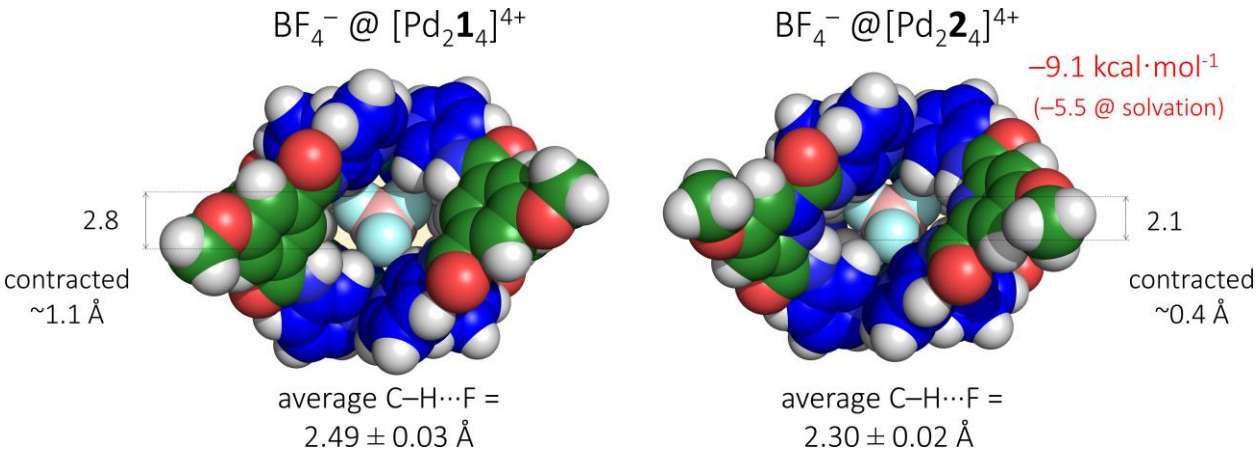

Figure S55. Comparison of the DFT-generated models of both cages bound to BF_4^-. The interior heights of the structures was calculated as described in the caption of Figure S54 and indicate that the cage with **1** contracted much more (~1.1 Å) than the cage with **2** (~0.4 Å) after binding BF_4^-. Also, the intermolecular C–H···F distances with the cages derived from **1** (2.49 Å) are –on average– 0.2 Å longer than in the cage with **2** (2.30 Å). Both geometrical data suggest that BF_4^- is more tightly bound by $[Pd_2\mathbf{2}_4]^{4+}$ (right) than by $[Pd_2\mathbf{1}_4]^{4+}$ (left). The adduct with $[Pd_2\mathbf{2}_4]^{4+}$ is also 9.1 kcal·mol^{-1} more stable when calculated in the gas phase. When using these geometries in an energy calculation with the COSMO explicit solvation model and a dielectric constant of 10.72 the energy difference is still –5.5 kcal·mol^{-1} in favour of $[Pd_2\mathbf{2}_4]^{4+}$. These models thus providing an additional rationale for the reduced binding properties of $[Pd_2\mathbf{2}_4]^{4+}$. All distances are in Å and the dielectric constant of 10.72 is the weighted average of dichloromethane (8.82) and dimethylsulfoxide (46.83) in the ratio of 95:5 employed.

References

[1] *Synthesis*, 2015, *47*(16), 2485-2495.
[2] *Angewandte Chemie International Edition,* 2021, DOI:10.1002/anie.202104924.
[3] *Analytical Biochemistry*, 1995, *231*, 374-382.
[4] *Angewandte Chemie International Edition*, 2005, *44*, 520-554.
[5] *Chemical Communications*, 2021, DOI: DOI:10.1039/D1CC02663A.